TECHNICAL MEMORANDUM

573

Aerosol analysis and forecast in the ECMWF Integrated Forecast System: Forward modelling

J.-J. Morcrette[1], O. Boucher[2], L. Jones[1], D. Salmond[1], P. Bechtold[1], A. Beljaars[1], A. Benedetti[1], A. Bonet[1], J.W. Kaiser[1], M. Razinger[1], M. Schulz[3], S. Serrar[1], A.J. Simmons[1], M. Sofiev[4], M. Suttie[1], A. Tompkins[1,5], A. Untch[1], and the GEMS-AER team

[1]European Centre for Medium-Range Weather Forecasts, Reading, UK
[2]Met Office, Exeter, UK
[3]Laboratoire des Sciences du Climat et de l'Environnement, Gif-sur-Yvette, France
[4]Finnish Meteorological Institute, Helsinki, Finland
[5]now with ICTP, Trieste, Italy

Research Department

To be submitted to *J. Geophys. Res.*

September 30, 2008

European Centre for Medium-Range Weather Forecasts
Europäisches Zentrum für mittelfristige Wettervorhersage
Centre européen pour les prévisions météorologiques à moyen terme

Series: ECMWF Technical Memoranda

A full list of ECMWF Publications can be found on our web site under:
http://www.ecmwf.int/publications/

Contact: library@ecmwf.int

European Centre for Medium-Range Weather Forecasts
Shinfield Park, Reading, RG2 9AX, England

J.-J. Morcrette[a 1], O. Boucher[b], L. Jones[a], D. Salmond[a], P. Bechtold[a], A. Beljaars[a], A. Benedetti[a], A. Bonet[a], J.W. Kaiser[a], M. Razinger[a], M. Schulz[c], S. Serrar[a], A.J. Simmons[a], M. Sofiev[d], M. Suttie[a], A. Tompkins[a,e], A. Untch[a], and the GEMS-AER team

[a]ECMWF, Shinfield Park, Reading, RG2 9AX, United Kingdom
[b]MetOffice, Fitzroy Road, Exeter, EX1 3PB, United Kingdom
[c]Laboratoire des Sciences du Climat et de l'Environnement, Gif-sur-Yvette, France
[d]Finnish Meteorological Institute, Helsinki, Finland
[e]now with ICTP, Strada Costiera 11, 34014 Trieste, Italy

Abstract

With the formal end, within the GEMS project, of the period of development of the forward forecast model including aerosol processes, this report presents the state of the aerosol modelling in the ECMWF Integrated Forecasting System (IFS). It details the various parametrisations used in the IFS to account for the presence of tropospheric aerosols. Details are given of the various formulations and data-sets for their sources and of the parametrisations describing the sinks. Comparisons of monthly mean and daily aerosol quantities like optical depths against satellite and surface observations are presented. The capability of the forecast model to simulate aerosol events is illustrated through comparisons of dust plume events.

[1]Corresponding author: Jean-Jacques Morcrette, email: Morcrette@ecmwf.int

1. Introduction

In April 1989, the ECMWF model was the first operational forecast model to include the effects of aerosols as part of its radiation transfer calculations (from the initial work of Tanré et al., 1984 in a climate version of the model). Since then, a revised climatology (Tegen et al., 1997) was introduced in October 2003, and various studies (Tompkins et al., 2005; Rodwell, 2005) showed the positive impact of this change on various aspects of the model, sometimes far from the location of the main change in aerosol optical thickness.

As part of the project Global and regional Earth-system Monitoring using Satellite and in-situ data (GEMS, Hollingsworth et al., 2008), the European Centre for Medium-range Weather Forecasts (ECMWF) is developing its assimilation system to include observations pertaining to greenhouse gases, reactive gases and aerosols. For the computation of the trajectory forecast used in the assimilation, the Integrated Forecast System (IFS) has been extended to include a number of tracers, which are advected by the model dynamics and interact with the various physical processes. With respect to the aerosols, sources have thus been added to the model, and a representation of the aerosol physical processes (namely the interactions of the aerosols with the vertical diffusion and the convection, plus the sedimentation, dry deposition and wet deposition by large-scale and convective precipitation) are now part of the package of physical parametrisations of the ECMWF IFS model.

A prognostic representation of aerosols is a feature of numerous climate models (see Textor et al., 2006, for a review). However, it is more of a novelty in global weather forecast models, given the requirements on the assimilation system to deal properly with the aerosol-relevant observations. As part of the GEMS project, aerosol-related observations (whether aerosol retrievals or aerosol-sensitive radiances) will be assimilated together with all the other observations in a fully interactive way. Apart from these analyses including the aerosols, another objective is to have a combined meteorological and aerosol forecast. Given the final requirement of having not only the direct version of the aerosol routines, but also the tangent-linear and adjoint versions of the same aerosol routines of the model for use in the four-dimensional variational assimilation, a certain level of simplification has to be considered when accepting an existing parametrisation from the literature or designing a new one for the model. In this respect, the emphasis is somewhat different from that of the representation of aerosols in a general circulation model used for climate studies where aerosol processes may have a sophisticated representation in order to be able to handle various sensitivity studies. Here, the forecast model including aerosols will be used at relatively high resolution, both horizontally and vertically, to provide information on the aerosol loading over the time-scale of a few hours to a few days. In consequence, the dynamical transport becomes primordial in such forecasts, including the possibility of backward trajectories to determine, for example, the origin of the aerosols over a given point at a given time. It is therefore important to simulate the aerosol loading (and in the future, aerosol radiative forcing and possible impact of aerosols on clouds) on a monthly mean time scale, but it is even more important that the correct monthly means are obtained from an accurate representation of the short-term variability of the aerosol distributions.

Section 2 gives an overview of how the aerosols are introduced in the ECMWF IFS, with more attention given to the aerosol sources including some alternative parametrisations and data-sets that were tested during the development of the ECMWF aerosol model. Section 3 focuses on the representation of the sink terms. In section 4, comparisons of monthly mean optical depths at 550 nm against equivalent quantities derived from satellite observations (MODerate resolution Imaging Spectrometer, MODIS (Remer et al., 2005) and Multi-angle Imaging SpectroRadiometer, MISR (Kahn et al., 2005) are first presented. Then the representation of the day-to-day variability of the modelled aerosols is assessed through comparisons with surface measurements at AERONET (AErosol RObotic NETwork, Holben et al., 1998) sites. Finally, results of forecasts of meteorological events when a heavy aerosol load was prevalent are presented, together with optical depths at wavelengths other than 550 nm. Conclusion and perspectives are given in Section 5.

2. Model environment and aerosol sources

In the following, all mentions of the ECMWF model refer to the cycle 32R2 version of the library, operational from 5 June 2007 to 5 November 2007, set up for a T_L159 horizontal resolution (a grid of $[1.125^\circ]^2$ in the tropics) and either 60 vertical levels over the period December 2002-May 2005 or 91 levels for the near-real time simulations started on 15 May 2007. Within the model dynamics, some dedicated fields allow the advection of tracers to be properly handled in a way consistent with the rest of the dynamics. Over the past 15 years, a number of transport and climate models have included a representation of aerosol processes and an abundant literature exists on most details of their parametrisation (see Textor et al., 2006 for an overview and a recent list of references). Here, we only reference the main approaches for these various parametrisations and only detail those being introduced within the ECMWF model. Since 2005, developments in the ECMWF physical package have allowed the vertical diffusion and the mass-flux convection schemes to account explicitly for tracers, including aerosols. The wet and dry deposition schemes were directly adapted from the LOA/LMD-Z model (Reddy et al., 2005), whereas the sedimentation of aerosols follows closely what has been done for ice particles by Tompkins (2005). Details on the sources and other aerosol-related physical processes are given below. A diagram showing how the ECMWF IFS physical package has been updated to deal with the prognostic aerosols is given in Figure 1.

a. Model environment

The initial package of ECMWF physical parametrisations dedicated to aerosol processes mainly follows the aerosol treatment in the LOA/LMD-Z model (Boucher et al., 2002, Reddy et al., 2005). Five types of tropospheric aerosols are considered: sea salt, dust, organic and black carbon, and sulphate aerosols. A prognostic representation of the stratospheric aerosols is not included here, as the period 2003-2004 considered for the initial model development was almost devoid of any sizeable amount of stratospheric aerosols (at least, from a radiative point of view). Similarly, the emission of aerosols by volcanoes is not present in the following results. Both types of aerosols will be considered in a later stage of the GEMS-Aerosol project.

For all tropospheric aerosols, sources are defined, the sedimentation of all particles, and the wet and dry deposition processes are represented. In addition, the transfer from hygrophobic to hygrophilic, specific to organic matter and black carbon aerosols, is also included.

A bin representation is used in this study to include prognostic aerosols of natural origin (sea-salt SS and dust DU). From the start of the GEMS-Aerosols project, it had been decided to allow the maximum flexibility regarding the limits of the bins for the sea-salt and dust aerosols. In the following, the sea-salt aerosols are tentatively represented by 3 bins, with limits at 0.03, 0.5, 5 and 20 microns. Similarly, the desert dust aerosols are represented by 3 bins with limits at 0.03, 0.55, 0.9, and 20 microns. The above limits are chosen so that roughly 10, 20 and 70 percent of the total mass of each aerosol type are in the various bins.

For organic matter (OM) and black carbon (BC), two components, hygrophobic and hygrophilic, are considered. Sulphate (SO_4)is considered as one variable with no explicit chemistry included.

b. Aerosol sources.

In the ECMWF IFS, the two natural aerosols (SS and DU) have their sources only linked to some prognostic and diagnostic model variables. In contrast, the anthropogenic aerosols (OM, BC, SO_4) have their sources read from external data-sets. Sources of sea-salt and desert dust are interactive with surface and near-surface variables of the model.

Recently, the importance of accounting for gustiness in the surface wind used for diagnosing the surface flux of particles was stressed by Engelstaedter and Washington (2007). However, in the following, we present results obtained for sea salt and dust surface flux formulations using plain 10-m wind. The 10-m wind for April 2003 is presented in Figure 2, separately over the ocean and continental surfaces.

1) SEA SALT

Different approaches to sea salt production are reviewed in Guelle et al. (2001) and a detailed description of the processes involved is given in Grini et al. (2002). They include the generation of sea spray by wind stress on the ocean surface, either from air bubbles in the whitecaps, or at higher wind speeds, from spume drops torn directly from the wave crests (Smith et al., 1993).

Original source of sea-salt: Monahan et al., 1986

The vertical flux F_0 of sea salt aerosols is parametrised from the 10-meter wind at the free ocean surface following Monahan et al. (1986)

$$\frac{dF_0}{dr} = 1.373\ u_{10}^{3.41}\ r^{-3}\ (1+0.057r^{1.05})\ 10^{1.19e^{-B^2}} \tag{1}$$

where $B = (0.380 - \ln r)/0.650$, r is the particle radius (in μm) and u_{10} the 10-m wind speed (in ms^{-1}). The emission flux F_i (in particles $m^{-2}\ s^{-1}$) for a size bin (i) is obtained by integrating (2) over the size range $(r_{i1}$ to $r_{i2})$ in the bin to yield

$$F_i(u_{10}) = a_i u_{10}^{3.41} \tag{2}$$

where

$$a_i = \int_{r_{i1}}^{r_{i2}} 1.373 r^{-3}(1+0.057r^{1.05})\ 10^{1.19e^{-B^2}}\ dr \tag{3}$$

A density of 2160 kgm^{-3} is assumed for dry particles. Sea salt production is calculated assuming a 80 percent relative humidity. At this relative humidity, the particle radius will be twice the dry radius (Fitzgerald, 1975), and the density used in the production is thus 1182 kgm^{-3}. The number of particles produced is converted to mass according to

$$M = \frac{4\pi N \rho_p r^3}{3} \tag{4}$$

where M is the total mass produced in a model grid cell (kg), N is the total number produced, ρ_p is the particle density, and r is the radius.

Only the dry mass is added to the bin and transported. Thus no water is transported via the aerosols. Mass is not transferred between bins because of growth. However, wet density and radius are considered for all the size bins when dealing with dry deposition, sedimentation and radiation.

LSCE source for sea-salt: Schulz et al., 2004

The source function described above was initially tested in the IFS ("second aerosol simulation": eupr). For the extended simulation ("third aerosol simulation": exlz), the surface flux of sea salt is diagnosed using the source function developed at LSCE. This later source function is based on Guelle et al. (2001) and Schulz et al. (2004).

Similar source functions have been proposed by Vignati et al. (2001) and Grini et al. (2002). All these studies suggest to combine different source functions if one is interested in a wider aerosol size range. Wet sea salt mass fluxes at 80% relative humidity are integrated for the three size bins discussed above, merging Monahan et al. (1986) and Smith and Harrison (1998) between 2 and 4 μm. Figure 3 presents the source of sea salt aerosols averaged over April 2003, showing maximum emission over the Northern and Southern Hemisphere storm tracks.

FMI source for sea-salt

Another source function developed at the Finnish Meteorological Institute was also tested. Compared to the two previous ones, it accounts explicitly for the water temperature and salinity. Given that the model does not carry water salinity, that the formulation is much more computer-intensive and that the resulting sea salt surface flux is intermediate between the two other formulations, in the following, we only discuss results obtained with the LSCE formulation.

2) DUST

Dust mobilization is sensitive to a wide range of factors including soil composition, soil moisture, surface conditions and wind velocity. Dust uplifting into the atmosphere is mainly initiated by saltation bombardment (sand blasting). Various parametrisations have been developed over the years to represent these processes (Gillette et al., 1980; Tegen and Fung, 1994; Ginoux et al., 2001). Marticorena and Bergametti (1995) developed a sophisticated parametrisation of this process, which requires detailed information on soil characteristics, which is not readily available in the ECMWF global model.

For the production of desert dust in the ECMWF model, a formulation of the source was implemented following Ginoux et al. (2001). First, the areas likely to produce dust are diagnosed for snow-free land with at least 10 percent of bare soil, and the soil moisture below the wilting point. For these areas, the dust flux is a function of the surface wind

$$F_i(u_{10}) = \begin{cases} S u_{10}^2 (u_{10} - u_t) & \text{if } u_{10} > u_t \\ 0 & \text{otherwise} \end{cases} \quad (5)$$

where u_t is a lifting threshold speed depending on soil wetness and particle radius and S is the source function ($S = 2$ x$10^{-11} kg\ s^2 m^{-5}$). The main difference with the approach of Marticorena and Bergametti (1995) is that S, also called dust emission potential, is here independent of the soil morphology, and we rely on the 10-m wind, vegetation cover, soil moisture, (absence of) snow cover provided by the model and the MODIS-derived UV-visible component of the land surface albedo to diagnose which areas are likely to produce a flux of dust. Figure 4 presents the UV-visible albedo, moisture in the first soil layer, and the fraction of bare soil for April 2003. The corresponding sources of dust aerosols diagnosed with the formulation discussed above is shown in Figure 5.

3) ORGANIC MATTER, BLACK CARBON AND SULPHATE

Sources for the other aerosol types are taken from the GFED (Global Fire Emission Database), SPEW (Speciated Particulate Emission Wizard), EDGAR (Emission Database for Global Atmospheric Research) annual- or monthly-mean climatologies until more temporally-resolved data are provided as part of the GEMS project. Overall, these datasets include sources of organic and black carbon, and sulphate aerosols linked to fire emissions, both natural and anthropogenic, plus emissions from domestic, industrial, power generation, transport

and shipping activities. More details on the sources of aerosols can be found in Dentener et al. (2006). The data-sets used for the original model development were extracted from the AEROCOM emission inventories.

In the following, version 2 of the GFED dataset, given as 8-day means for the emissions of organic and black carbon, and sulphate aerosols is used. Figure 6 presents, averaged over April 2003, the difference in total aerosol optical depth at 550 nm (τ_{550}) using either GFED 8-day (fire emission data averaged over 8 days and relevant for the period of simulation) or the GFED climatology (based on monthly means for the year 2000). For April 2003, the effect of using a higher temporal resolution for emissions is seen over South-Eastern Russia and west of Central America.

3. Removal processes.

Several types of removal processes are considered, the dry deposition including the turbulent transfer to the surface and the gravitational settling, and the wet deposition including rainout (by large-scale and convective precipitation) and washout of aerosol particles in and below the clouds. The wet and dry deposition schemes are standard, whereas the sedimentation of aerosols follows closely what was recently introduced for the sedimentation of ice particles. Hygroscopic effects are also considered here.

a. Dry deposition.

The turbulent transfer of particles at the surface is represented as a decrease in the emission flux represented through a deposition velocity v_d. A review of the knowledge on dry deposition, taking into account the surface type (ocean or land, vegetation type) is given by Wisely and Hicks (2000). In these preliminary results, the dry deposition to the surface is accounted for through a decrease of the aerosol concentration in the lowermost model layer assuming a flux

$$F_{DD} = C v_d \tag{6}$$

where C is the concentration in the first layer above the surface (in gm^{-3}), v_d is the dry deposition velocity, simply function of the particle mode radius and surface type. More sophisticated representations would make v_d depend on the aerodynamic resistance r_a and the resistance in the quasi-laminar sub-layer r_b, linking it to either the vegetation or the wave characteristics.

b. Sedimentation.

For the larger aerosols, the most efficient removal process is the gravitational settling (sedimentation). The change in concentration follows the approach developed by Tompkins (2005) for the sedimentation of ice. For a concentration C, including a flux form term for transport at a velocity v_s, the change in concentration is given by

$$\frac{dC}{dt} = \frac{1}{\rho}\frac{d(\rho v_s C)}{dz} \tag{7}$$

Tompkins (2005) shows that the solution is

$$C_j^{n+1} = \frac{\frac{\rho_{j-1} v_{j-1} C_{j-1}^{n+1}}{\rho_j \Delta Z} \Delta t + C_j^n}{1 + \frac{\rho_{j-1} v_j}{\rho_j \Delta Z} \Delta t} \tag{8}$$

which is solved from top to bottom of the column.

The settling velocity v_s for a particle of radius r is determined by Stokes's law

$$v_s = \frac{2\rho_p g}{9\mu} r^2 C_{Cunn} \tag{9}$$

where ρ_p is the particle density, g the acceleration of gravity, μ is the absolute viscosity of air, and C_{Cunn} is the Cunningham correction to account for the viscosity dependency on air pressure and temperature.

c. Hygroscopic effects on carbonaceous compounds

Black carbon and organic matter aerosols are produced from the sources discussed in Section 2.3. From those sources, the organic matter (OM) is distributed between 50 percent of hydrophilic and 50 percent of hydrophobic OM, where as for black carbon (BC), 80 percent is kept as hydrophobic and 20 percent is considered as hydrophilic BC. Once emitted, the hydrophobic component is transformed into a hydrophilic one with a time constant of 1.16 day. This follows a similar parametrization in the LOA/LMD-Z model.

d. Conversion SO_2 / SO_4

Sulphur dioxide SO_2 is produced at or near the surface as discussed in Section 2.3. The transformation of SO_2 into sulphate SO_4 is done without any explicit chemistry. The exponential transfer from SO_2 and SO_4 uses a simple time constant, itself a variable with latitude, as done in the simplified aerosol model of Huneeus (2007).

e. Wet deposition.

A review of GCM-type schemes to deal with wet precipitation scavenging can be found in Lee and Feichter (1995) and Rasch et al. (2000). In this study, wet deposition is computed separately for convective and large-scale precipitation using the relevant precipitation flux profiles, and following Giorgi and Chameides (1986) for the in-cloud scavenging.

The scavenging rate (s^{-1}) is given by $W_I = \beta f r$, with r the fraction of aerosol included in droplets through dissolution or impaction, f the cloud volume fraction, and β the rate of conversion of cloud water to rainwater (in $kgkg^{-1}s^{-1}$). r is set to 0.7 for both sea salt and desert dust. The parameter β at model level k is computed from the 3D precipitation flux P (in $kgm^{-2}s^{-1}$) and the model condensed in-cloud water mixing ratio q (in $kgkg^{-1}$) as

$$\beta_k = \frac{P_k - P_{k+1}}{\rho_{air,k} \Delta z_k f_k q_k} \tag{10}$$

In these preliminary results, as in Reddy et al. (2005), no distinction is made between rain and snow and f is assumed to represent the cloud fraction over the full vertical layer.

Below-cloud scavenging is computed considering the volume of space swept by a raindrop during its fallout. The scavenging rate is given by

$$W_B = \frac{3P_r\alpha}{4R_r\rho} \tag{11}$$

where R_r is an average raindrop radius (set to 1mm), ρ the water density (kgm^{-3}) and α the efficiency with which aerosols are collected by raindrops. Values of 0.001 and 0.01 for raindrops and snowflakes were selected for α based on measurements reported in Pruppacher and Klett (1997).

The release at a level k is equal to the amount scavenged at higher levels multiplied by the fraction of precipitation which is evaporated, with an 0.5 multiplicative factor to account for the fact that raindrops can shrink without evaporating totally. If the incoming precipitation flux totally evaporates in the layer, the aerosols are released totally as well.

4. Results

For the results presented below, there is **no** assimilation of any data related to aerosol. The model, including the parametrisations for the physical aerosol processes discussed in sections 2 and 3, was run from a given initial date in a series of 12-hour forecasts starting every 12 hours from the ECMWF operational analyses. The model aerosols are free-wheeling, i.e., starting from null concentrations of aerosols on the initial date, the various aerosols are let to spin up for about 8-12 days (the time their contents establish themselves) with aerosols produced from surface emission fluxes, and going through the physical processes (dry deposition, sedimentation, hygroscopicity, wet deposition by large-scale and convective precipitation). The aerosols at the end of a given 12-hour forecast are passed as initial conditions at the start of the next 12-hour forecast. This is in essence not very different from what is done within a transport model, except for the fact that the aerosol processes are consistent with the dynamics and all other physical parametrizations.

Two sets of forecasts were conducted. The first one (exlz), directly part of the GEMS project, is a series of 12-hour forecasts at $T_L159L60$ covering the period 1 December 2002 00UTC to 31 May 2005 24UTC. The second one (f0dm) includes experimental near-real time 72-hour forecasts at $T_L159L91$ started on 15 May 2007 00UTC and going on since.

Although in this stage of the development of the ECMWF IFS, the aerosols are not interactive with the radiation scheme, the optical thicknesses for all aerosols are evaluated as diagnostic quantities that can be compared to measurements such as those taken by AERONET (Holben et al., 1998; Dubovik et al., 2002; Kinne et al., 2003), or derived from satellite measurements like those of MODIS (Remer et al., 2005).

a. Observational datasets

Various sources of observational data have been used to verify the model aerosols. Satellite observations as carried out by MODIS (MODerate resolution Imaging Spectroradiometer) on the Terra and Aqua satellites provide optical depth at 550 nm (τ_{550}) each once a day over a wide path. MISR (Multi-angle Imaging SpectroRadiometer) on-board Terra provides the aerosol optical depth at 557.5 nm in similar conditions, but with a coarser spatial coverage. Figure 7 displays for April 2003 the monthly mean aerosol optical depth at 550 nm from MODIS on Terra, MODIS on Aqua (Remer et al., 2005) and MISR (kahn et al., 2005) on Aqua, with Figure 8 showing the difference in monthly mean τ_{550} between MODIS on Terra and Aqua. First, Figure 7 shows that τ_{550} is not retrieved at high latitudes when the solar illumination is small, nor over bright surfaces (snow over

Northern hemisphere high latitudes or the desert areas of Sahara and Australia). MISR τ_{557} displays a similar (but noisier) geographical distribution of aerosol as MODIS, with some suspicious features over high-latitude snow-covered areas.

As shown in Figure 8, although the differences are not systematic and may be due to different overpass times in some regions, there appears to be an uncertainty of $\pm$ 0.05 on τ_{550} over a large fraction of the ocean. These differences are less extended over land.

The CALIPSO lidar on the Aqua satellite provides vertical profiles of the aerosol extinction coefficient along the satellite track over a narrow track whereas the radar on-board CloudSat provides a similar information on clouds (Stephens et al., 2002). In the following, the vertical distribution of aerosols and clouds along the A-Train track within the ECMWF IFS is qualitatively compared to the cloud-aerosol mask derived from combined CloudSat-CALIPSO observations.

AERONET is a federated network of ground stations measuring the solar radiation over a number of wavelengths (Holben et al., 1998). In absence of overlying cloudiness, these measurements are processed to give the aerosol optical depth. For validating the model aerosols, a number of stations (41 in April 2003) spanning the whole globe are used to compare the model optical depth at 550 nm with the observed optical depth (at 500 nm).

b. Model aerosol optical properties

Aerosol optical depth is diagnosed for the 17 shortwave wavelengths given in Table 1. The refractive indices were derived from Lacis (2001) for sea salt and interpolated from Dubovik et al. (2002) for desert dust. Then a standard Mie scattering algorithm is applied using, for sea salt and dust aerosols, the particle size distribution as simulated by the bin scheme but also accounting for a fixed size distribution within each bin that has been calibrated against a model with more bins. Optical depth for sea salt and dust are obtained by summing the individual bin contribution to the optical thickness for each aerosol type. Absorption and scattering coefficients for organic and black carbon, and sulphate were adapted from those in the LOA/LMD-Z model (Reddy et al., 2005).

λ (nm)	Observation type	Instrument
340	τ	AERONET
380	τ, extinction	AERONET, SAGE-3
400	τ	SEVIRI
443	τ	AERONET (440), MISR (446)
470	τ, reflectance	MODIS (469) (land/ocean)
500	τ	AERONET
532	backscatter coefficient	CALIOP
550	τ, reflectance	MODIS (555), MISR (557)
645	τ, reflectance	MODIS (645) (land/ocean)
670	τ, extinction	MISR (672), AERONET (675), SAGE-3 (676)
800	τ	SEVIRI
858	τ, reflectance	MODIS (land/ocean)
865	extinction, τ	MISR (867), SAGE-3 (868)
1020	extinction, backscatter coefficient, τ	SAGE 3, CALIOP (1064), AERONET
1240	τ, reflectance	MODIS (ocean)
1630	τ, reflectance	MODIS (ocean)
2130	τ, reflectance	MODIS (land/ocean)

Table 1: Satellite observations simulated by the ECMWF IFS with prognostic aerosols.AERONET, MISR and SEVIRI provide optical depth τ, MODIS provides reflectance and τ, CALIOP provides profiles of the backscattering coefficient, SAGE-3 provides extinction coefficient.

c. Monthly-mean total aerosol optical depth

Figure 9 compares the total aerosol optical depth averaged over April 2003, derived from MODIS on Terra to the one produced by the ECMWF IFS. A number of features of the aerosol distribution are present, namely the desert dust over Sahara, anthropogenic aerosols over Eastern Europe, South India and Eastern China, effect of fires in Mexico. However, the comparison between the model and the MODIS observations also shows too large τ_{550} over the Southern hemisphere storm track (likely to be linked to too large production of sea salt aerosols), too little τ_{550} over Central Africa (biomass burning), Central America and downwind of Asia.

Comparing the model τ_{550} to the AERONET τ_{500} on a monthly mean basis (for April 2003), Figure 10 further points out a deficit of aerosols in Northern and Eastern Europe, Saudi Arabia and Northern India (between -0.025 and -0.25) and a large one for the Arica station (Northern Chile) where aerosols linked to copper smelters are not well represented in the emission datasets. Although from theoretical considerations, τ_{550} can be expected to be slightly smaller than τ_{500}, the difference in wavelength cannot explain the differences between model and AERONET observations.

It is also to be noticed that as for satellite observations, ground observations of aerosols in the short-wave spectrum are very scarce at high latitudes with only a few observations during daytime in absence of cloudiness.

d. Time variability of the aerosol optical depth

Figure 11 presents the time evolution of the bias and r.m.s. error of the model total aerosol optical depth relative to a set of 41 AERONET stations over the globe, in Europe, Africa, South-East Asia and North America. The biases are generally negative (by 0.1 to 0.25 over S.E. Asia), showing an underestimation of τ_{550} in the model. The r.m.s. error is on average below 0.2 with much higher peaks corresponding to aerosol events, not seen by the model, usually because of sources not displaying increased emissions. For a number of individual stations where either sea salt, desert dust, or anthropogenic aerosols are dominating the total aerosol optical depth, Figures 12 to 14 display the evolution of the bias and r.m.s. error in τ_{550} relative to AERONET measurements and the corresponding MODIS optical depth, when available.

Figure 12 considers stations where sea salt aerosols are likely to be dominant (Amsterdam Island 37.81S-77.57E, Ascension Island 7.98S-14.42W, Azores 38.53N-28.63W, Nauru 0.52S-166.92E, Tahiti 17.58S-149.61W). Overall the agreement between model and observations is good with a proper representation of the temporal variability. Figure 13 presents similar comparisons for stations where dust aerosols are prevalent (Dahkla 23.72N-15.95W, Dalanzadgad 43.58N-104.42E, Forth Crete 35.53N-25.28E, Sede Boker 30.86N-34.78E, Solar Village 24.91N-46.40E). For these stations for which sudden increases in aerosol optical depth are linked to dust plumes, the agreement is also good, with a correct representation of the background aerosol optical depth and of the timing of the sudden increases. However, as can be seen particularly for Sede Boker and Solar Village, the amplitude of these events is generally underestimated by the model. Figure 14 considers comparisons over stations where anthropogenic aerosols dominate the total aerosol optical depth (Bondville 40.05N-88.37W, Hamburg 53.57N-9.97E, Moldova 47.00N-28.82E, Sao Paulo 23.56S-46.74W, Shirahama 33.69N-135.36E, Wallops 37.94N-75.47W). For these stations, even when the average optical depth over the month is reasonable, the model temporal variability only reflects the quality of the dynamics of the ECMWF IFS. If the sources of aerosols in upwind regions are reasonably represented (Bondville, Wallops), a proper timing of the fluc-

tuations in τ_{550} is seen. If the sources are not well included (either in timing or intensity of the emissions), either the fluctuations are out of phase (Sao Paulo, Shirahama) or the aerosol optical depth is underestimated (Hamburg, Moldova).

e. Vertical and horizontal distribution of the aerosol layers

Plumes of aerosols of desert origin are not uncommon over Europe. In April 2003, three such plumes were observed coming out of Africa. Figures 15 to 17 compare *qualitatively* the MODIS visible imagery and τ_{550}^{DU} for these three events on the 4^{th}, 15^{th} and 30^{th} of April 2003. In all cases, the model displays a plume of desert aerosols in the area of concern showing that, given a source of dust over Africa, the dynamics of the model is successful at distributing spatially the aerosols with the proper timing. However, the representation of the actual intensity of these events is much more difficult to capture, with, for example, too large an intensity on 4 April (Fig. 15) and too small on 15 (Fig. 16) and 30 April (Fig. 17).

Figure 18 illustrates the potential of the future aerosol forecasts, in terms of instantaneous vertical and horizontal distributions of aerosols. For an ascending orbit over Africa (Fig. 18a), a classification of cloud and aerosol produced by the CALIPSO Science Team (Fig. 18c) is compared with the corresponding model cloud and aerosol (Fig. 18d). Even for this relatively low horizontal resolution (T_L159), the ECMWF model generally produces the cloud and aerosol in the proper location both horizontally and vertically. Over the same orbit, the total aerosol optical depth at 550 nm produced by the model (Fig. 18b) is compared to the equivalent optical depth retrieved from MODIS observations over ocean and dark land surfaces in absence of extended cloud cover. For desert dust, the agreement is usually good reflecting the high quality of the initial conditions and of the atmospheric motions in the subsequent 12-hour forecast. Over Central Africa, the sources of sulphate, organic and black carbon aerosols linked to biomass burning are well represented in the inventories, and the agreement on the optical depth of the plume moving towards the South Atlantic is also good.

f. Multi-spectral optical depth diagnostics

The optical thickness in the seven MODIS short-wave channels is presented in Figure 19 as forecasted for July 2007 from the same aerosol simulation as in Fig. 18. As expected, different aerosol types, dominant in different locations, have a distinct spectral signature. The sea-salt aerosols (dominant in the Southern hemisphere storm track) display a rather flat spectral signature with almost no variation in optical thickness between 469 and 2130 *nm*. Desert dust aerosols (Sahara) show a steady decrease in optical thickness with increasing wavelength. Black carbon aerosols (Central Africa) display a rapid decrease from 469 to 865 *nm*, then keep a roughly constant value of optical thickness at longer wavelengths. These spectral characteristics will obviously help in the validation of the prognostic aerosols against multi-spectral surface and satellite measurements. This will also form the basis of the variational assimilation of aerosols using radiances, which will be tested, in the future, in the analysis part of GEMS-Aerosol.

5. Conclusions and perspectives

This report has presented the representation of tropospheric aerosols, now included in an experimental version of the ECMWF forecast system. It has detailed the various parametrisations introduced for dealing with the sources and sinks of the sea-salt, dust, organic matter and black carbon and sulphate aerosols. The quality or otherwise of the resulting aerosols has been documented through comparisons with monthly mean optical depths from MODIS and MISR, and from comparisons with time-series of optical depths at a number of AERONET sites. This report has concentrated on the forward model providing the trajectory calculations used

for the 4D-Var assimilation of aerosol-related observations discussed in Benedetti et al. (2008).

The experimental aerosol model discussed here is likely to undergo further developments. Such potential improvements will be reported elsewhere. However, the results presented here show that this version of the IFS including prognostic aerosols produces reasonable stand-alone forecasts and already offers a good starting point for the analysis of aerosol-related observations into the 4D-Var assimilation system. One of the priorities will be to unbias the forward model. Again, it has to be stressed that the forward model discussed here might not include all the sophistication encountered in some climate-orientated general circulation models including prognostic aerosols. The model presented here offers a good trade-off between the computer efficiency and the quality of the resulting aerosol fields, both required for use as forward model in an analysis scheme.

Since 15 May 2007, this experimental version of the forecast model including aerosols has been running at T_L159 L91 producing a near-real time aerosol forecast available from the ECMWF web site (see web address below).

The quality of the results of the forward model depends not only on the dynamics of the model and the adequacy of the aerosol physical parametrizations, but also on the representativeness of the sources. With the exact sources of aerosols (in particular, those of anthropogenic origin) not available in real time, the aerosol analysis, through the assimilation of aerosol-related observations, will provide initial conditions more representative of the true aerosol distribution in the atmosphere. The development of a successful aerosol analysis is therefore fundamental to the quality of the subsequent aerosol forecast. Here the forecast model including prognostic aerosols was shown to provide a reasonable basis for this analysis.

How succesful the model is at reproducing the temporal variability of the aerosol load depends mainly on the quality of the model dynamics. In that respect, the results indicate that the model advection is very dependable in describing the maxima and minima of the aerosol optical depth over most stations. Whether the overall amplitude of the model optical depth is consistent with what is observed depends for a large part on which aerosol type is dominant and when anthropogenic aerosols dominate the optical depth, on the quality of the information on the sources of aerosols.

The ECMWF model fields were compared to the equivalent fields compiled within the framework of AEROCOM (*http://nansen.ipsl.jussieu.fr/AEROCOM*), the Global Aerosol Model Intercomparison project. As discussed by Textor et al. (2006), even for the natural sea salt and desert dust aerosols, there is a wide diversity, not only in emission, but also in the partitioning between wet and dry deposition, and between gravitational settling and turbulent deposition. This results in a reasonable agreement between models as far as total optical thickness is concerned, but different distributions between aerosol types, as well as different vertical distributions of aerosols. At the end of this stage, the main message is that the ECMWF model can handle prognostic aerosols reasonably well, and be within the "accepted" diversity of the AEROCOM results.

Acknowledgements

This report is dedicated to the memory of Tony Hollingsworth whose vision and energy made the GEMS project possible. M. Schulz (LSCE) and M. Sofiev (FMI) provided routines for the emission of sea salt, some in a particularly user-friendly format. Comments by Y. Balkanski (LSCE), and discussions with G. Balsamo (ECMWF) helped define the various representations used in time for the emission of dust. L. Gonzalez (LOA, Univ. Lille) provided the MODIS imagery in Figures 15 to 17. Among the ECMWF authors of this report, P. Bechtold upgraded the convection scheme, A. Beljaars did the same for the vertical diffusion scheme, A. Bonet allowed the aerosol forecast to run in near-real time, L. Jones designed the plot package used for the validation at the AERONET stations and produced all the corresponding plots, J.W. Kaiser provided the 8-day sources for the anthropogenic aerosols and checked that the prognostic aerosols were working at all model resolutions, M.

Razinger produced the web environment to display the near-real time aerosol forecast, D. Salmond was of great help in debugging various versions of the aerosol codes, S. Serrar modified the model environnement to accept the new aerosol-related surface variables, M. Suttie made the MODIS data used for validation fit the ECMWF system. A. Tompkins produced the sedimentation routine, and A. Untch modified the dynamics of the model to handle the prognostic aerosols. R. Engelen is thanked for help in merging the prognostic aerosol model into successive versions of the operational IFS.

Surface observations were obtained from the AERONET web site. The MODIS, MISR and CALIPSO data were downloaded from the NASA Giovanni server.

References

AEROCOM emission inventory: http://nansen.ipsl.jussieu.fr/AEROCOM/

A-Train description: http://www.nasa.gov/mission_pages/cloudsat/multimedia/a−train.html

Benedetti, A., J.-J. Morcrette, O. Boucher, A. Dethof, R.J. Engelen, M. Fisher, H. Flentjes, N. Huneeus, L. Jones, J.W. Kaiser, S. Kinne, A. Mangold, M. Razinger, A.J. Simmons, M. Suttie, and the GEMS-AER team, 2008: Aerosol analysis and forecast in the ECMWF Integrated Forecast System: Data assimilation. *ECMWF Technical Memorandum*, **571**, 23 pp.

Boucher, O., M. Pham, and C. Venkataraman, 2002: *Simulation of the atmospheric sulfur cycle in the LMD GCM. Model description, model evaluation, and global and European budgets*. IPSL, Note 23, 26 pp. (available at http://www.ipsl.jussieu.fr/poles/Modelisation/NotesSciences.htm.)

Dentener, F., S. Kinne, T. Bond, O. Boucher, J. Cofala, S. Generoso, P. Ginoux, S. Gong, J. J. Hoelzemann, A. Ito, L. Marelli, J. E. Penner, J.-P. Putaud, C. Textor, M. Schulz, G. R. van der Werf, and J. Wilson, 2007: Emissions of primary aerosol and precursor gases in the years 2000 and 1750 prescribed data-sets for AeroCom. *Atmos. Chem. Phys.*, **6**, 4321-4344.
http://www.atmos-chem-phys.net/6/4321/2006/acp-6-4321-2006.pdf

Dubovik, O., B. Holben, T.F. Eck, A. Smirnov, Y.J. Kaufman, M.D. King, D. Tanré, and I. Slutsker, 2002: Variability of absorption and optical properties of key aerosol types observed in worldwide locations *J. Atmos. Sci.*, **59**, 590-608.

Engelstaedter, S. and R. Washington, 2007: Temporal controls on global dust emissions: The role of surface gustiness. *Geophys. Res. Lett.*, **34**, L15805, doi:10.1029/2007GL029971.

Fitzgerald, J.W., 1975: Approximation formula for the equilibrium size of an aerosol particle as a function of its dry size and composition, and the ambient relative humidity. *J. Appl. Meteorol.*, **14**, 1044-1049.

GEMS-AER experimental near-real time aerosol forecast: http://gems.ecmwf.int/d/products/aer/realtime/

GEMS-AER comparisons with AERONET: http://gems.ecmwf.int/d/products/aer/verif/exlz-ezub/

Gillette, D.A., J. Adams, A. Endo, and D. Smith, 1980: Threshold velocities for input of soil particles in the air by desert soils. *J. Geophys. Res.*, **85**, 5621-5630.

Ginoux, P., M. Chin, I. Tegen, J. Prospero, B.N. Holben, O. Dubovik, and S.-J. Lin, 2001: Sources and distributions of dust aerosols simulated with the GOCART model. *J. Geophys. Res.*, **106D**, 20255-20274.

Giorgi, F., and W.L. Chameides, 1986: Rainout lifetimes of highly soluble aerosols and gases as inferred from simulations with a general circulation model. *J. Geophys. Res.*, **91D**, 14367-14376.

Grini, A., G. Myhre, J.K. Sundet, and I.S.A. Isaksen, 2002: Modeling the annual cycle of sea salt in the global 3D model Oslo CTM2: Concentrations, fluxes and radiative impact. *J. Climate*, **15**, 1717-1730.

Guelle, W., M. Schulz, Y. Balkanski and F. Dentener, 2001: Influence of the source formulation on modelling the atmospheric global distribution of the sea salt aerosol. *J. Geophys. Res.*, **106D**, 27509-27524.

Holben, B.N., T.F. Eck, I. Slutsker, D. Tanré, J.P. Buis, A. Setzer, E. Vermote, J.A. Reagan, Y.J. Kaufman, T. Nakajima, F. Lavenu, I. Jankowiak, A. Smirnov, 1998: An emerging ground-based aerosol climatology: Aerosol optical depth from AERONET. *J. Geophys. Res.*, **103D**, 12067-12097

Hollingsworth, A., R.J. Engelen, C. Textor, A. Benedetti, O. Boucher, F. Chevallier, A. Dethof, H. Elbern, H. Eskes, J. Flemming, C. Granier, J.W. Kaiser, J.-J. Morcrette, P. Rayner, V.-H. Peuch, L. Rouil, M.G. Schultz, A.J. Simmons, and the GEMS Consortium, 2008: The Global Earth-system Monitoring using Satellite and in-situ data (GEMS) project: Towards a monitoring and forecasting system for atmospheric composition. *Bull. Amer. Meteor. Soc.*, **89**, 1147-1164, doi: 10.1175 /2008BAMS2355.1

Huneeus, N., 2007: Assimilation variationnelle d'observations satellitaires dans un modéle atmosphérique d'aérosols, *These de l'Universite des Sciences et technologies de Lille*, 225 pp.

Kinne S., et al., 2003: Monthly averages of aerosol properties: A global comparison among models, satellite data, and AERONET ground data, *J. Geophys. Res.*, **108D**, 4634, doi: 10.1029 /2001JD001253.

Lee, H.N., and H. Feichter, 1995: An intercomparison of wet precipitation scavenging schemes and the emission rates of ^{222}Rn for the simulation of global transport and deposition of ^{210}Pb. *J. Geophys. Res.*, **100D**, 23253-23270.

Marticorena, B., et G. Bergametti, 1995: Modelling the atmospheric dust cycle. 1: Design of a soil-derived dust emission scheme. *J. Geophys. Res.*, **100D**, 16,415-16,430.

Monahan, E.C., K.L. Davidson and D.E. Spiel, 1982: Whitecap aerosol productivity deduced from simulation tank measurements. *J. Geophys. Res.*, **87**, 8898-8904.

Pruppacher, H.R., and J.D. Klett, 1997: *Microphysics of Clouds and Precipitation*, 2nd revised and enlarged Ed., Kluwer Academic Publ., Boston, Mass., 954 pp.

Rasch, P.J., J. Feichter, K. Law, N. Mahowald, J. Penner, et al., 2000: An assessment of scavenging and deposition processes in global models: Results from the WCRP Cambridge workshop of 1995. *Tellus*, **52B**, 1025-1056.

Reddy M. S., O. Boucher, N. Bellouin, M. Schulz, Y. Balkanski, J.-L. Dufresne, M. Pham, 2005: Estimates of global multicomponent aerosol optical depth and direct radiative perturbation in the Laboratoire de Meteorologie Dynamique general circulation model, *J. Geophys. Res.*, **110D**, S16, doi: 10.1029 /2004JD004757.

Remer, L.A., Y.J. Kaufman, D. Tanré, S. Mattoo, D.A. Chu, J.V. Martins, R.-R. Li, C. Ichoku, R.C. Levy, R.G. Kleidman, T.F. Eck, E. Vermotte, and B.N. Holben, 2005, The MODIS aerosol algorithm, products and validation. *J. Atmos. Sci.*, **62**, 947-973.

Rodwell, M., 2005: The local and global impact of the recent change in model aerosol climatology. *ECMWF Newsletter*, **105**, 17-23.

Schulz, M., G. de Leeuw, and Y. Balkanski, 2004: Sea-salt aerosol source functions and emissions. in *Emission of Atmospheric Trace Compounds*, C. Granier, P. Artaxo and C.E. Reeves, eds. Kluwer, 333-354.

Smith, M.H., P.M. Park, and I.E. Consterdine, 1993: Marine aerosol concentrations and estimated fluxes over the sea. *Quart. J. Roy. Meteor. Soc.*, **119**, 809-824.

Smith, M.H. and N.M. Harrison, 1998: The sea spray generation function. *J. Aerosol Sci.*, **29**, Suppl.1, S189-S190.

Stephens, G.L. and Coauthors, 2002: The Cloudsat mission and the A-Train. *Bull. Amer. Meteor. Soc.*, **83**, 1771-1790.

Tanré, D., J.-F. Geleyn, and J.M. Slingo, 1984: First results of the introduction of an advanced aerosol-radiation interaction in the ECMWF low resolution global model, in *Aerosols and their Climatic Effects*, H.E. Gerber and A. Deepak, eds., A. Deepak Publishing, Hampton, Va, USA, 133-177.

Tegen, I., and I. Fung, 1994: Modeling of mineral dust in the atmosphere: Sources, transport and optical thickness. *J. Geophys. Res.*, **99D**, 22897-22914.

Tegen, I, P. Hoorig, M. Chin, I. Fung, D. Jacob, and J. Penner, 1997: Contribution of different aerosol species to the global aerosol extinction optical thickness: Estimates from model results. *J. Geophys. Res.*, **102**, 23,895-23,915.

Textor, C., M. Schulz, S. Guibert, S. Kinne, Y. Balkanski, S. Bauer, T. Berntsen, T. Berglen, O. Boucher, M. Chin, F. Dentener, T. Diehl, R. Easter, H. Feichter, D. Fillmore, S. Ghan, P. Ginoux, S. Gong, A. Grini, J. Hendricks, L. Horowitz, P. Huang, I. Isaksen, T. Iversen, S. Kloster, D. Koch, A. Kirkevåg, J.E. Kristjansson, M. Krol, A. Lauer, J.F. Lamarque, X. Liu, V. Montanaro, G. Myhre, J. Penner, G. Pitari, S. Reddy, Ø. Seland, P. Stier, T. Takemura, and X. Tie, 2006: Analysis and quantification of the diversities of aerosol life cycles within AeroCom. *Atmos. Chem. Phys.*, **6**, 1777-1813.

Tompkins, A.M., 2005: A revised cloud scheme to reduce the sensitivity to vertical resolution. *ECMWF Research Dept Technical Memorandum*, **0599**, 25 pp.

Tompkins, A.M., C. Cardinali, J.-J. Morcrette, and M. Rodwell, 2005: Influence of aerosol climatology on forecasts of the African Easterly Jet. *Geophys. Res. Letters*, **32**, L10801, doi: 10.1029 /2004GL022189.

Vignati, E., G. de Leeuw, and R. Berkowicz, 2001: Modeling coastal aerosol transport and effects of surf-produced aerosols on processes in the maritime atmospheric boundary layer. *J. Geophys. Res.*, **106**, 20225-20238.

Wisely, M.L., and B.B. Hicks, 2000: A review of the current status of knowledge on dry deposition. *Atmos. Environ.*, **34**, 2261-2282.

List of Figures

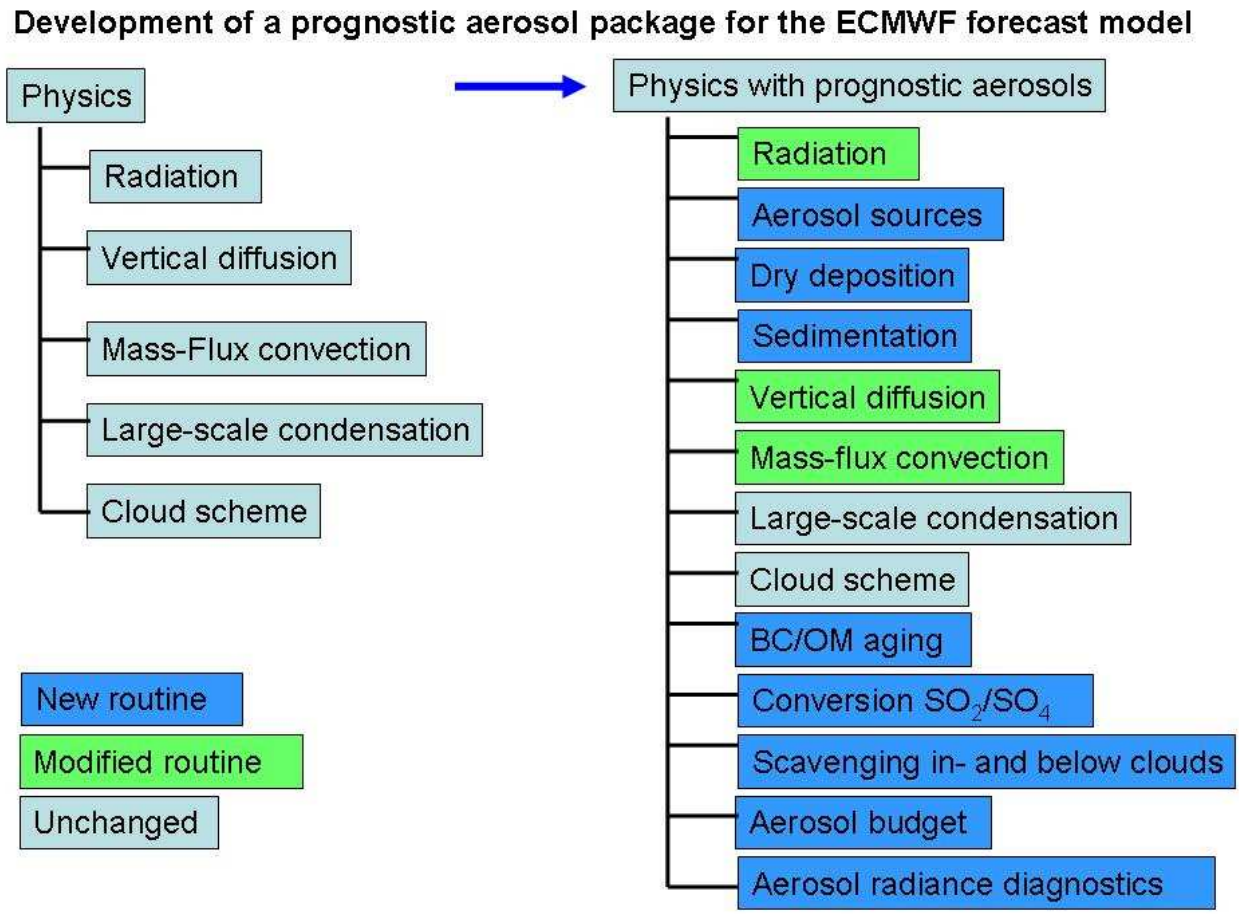

FIG. 1. Comparison of calling sequence for the physics without and with routines for prognostic aerosols. Left column: without. Right column: with.

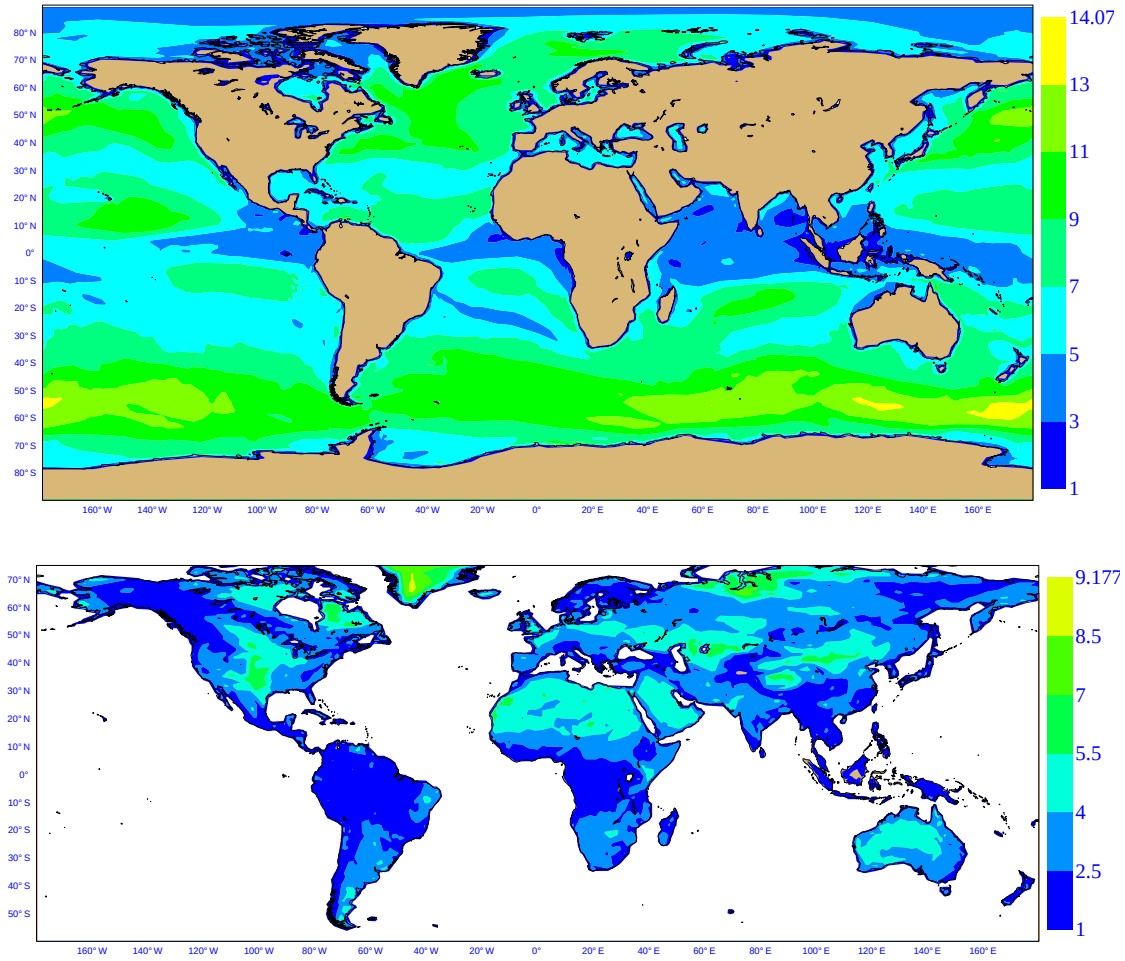

FIG. 2. The wind at 10 metres over ocean (top panel) and land (bottom panel) for April 2003 (in ms^{-1}).

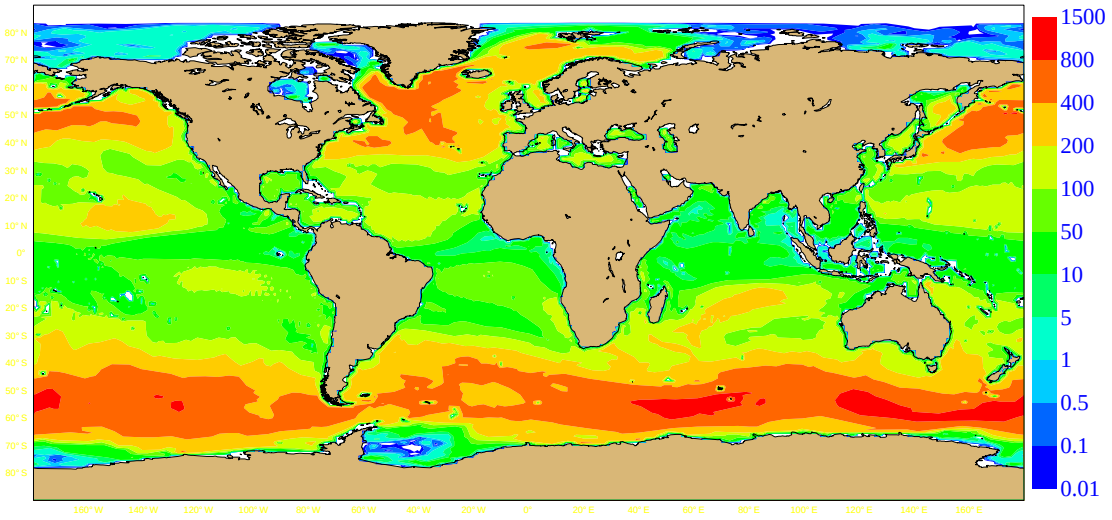

FIG. 3. The source of sea salt aerosols for April 2003 with the LSCE formulation (in units of $gm^{-2}year^{-1}$).

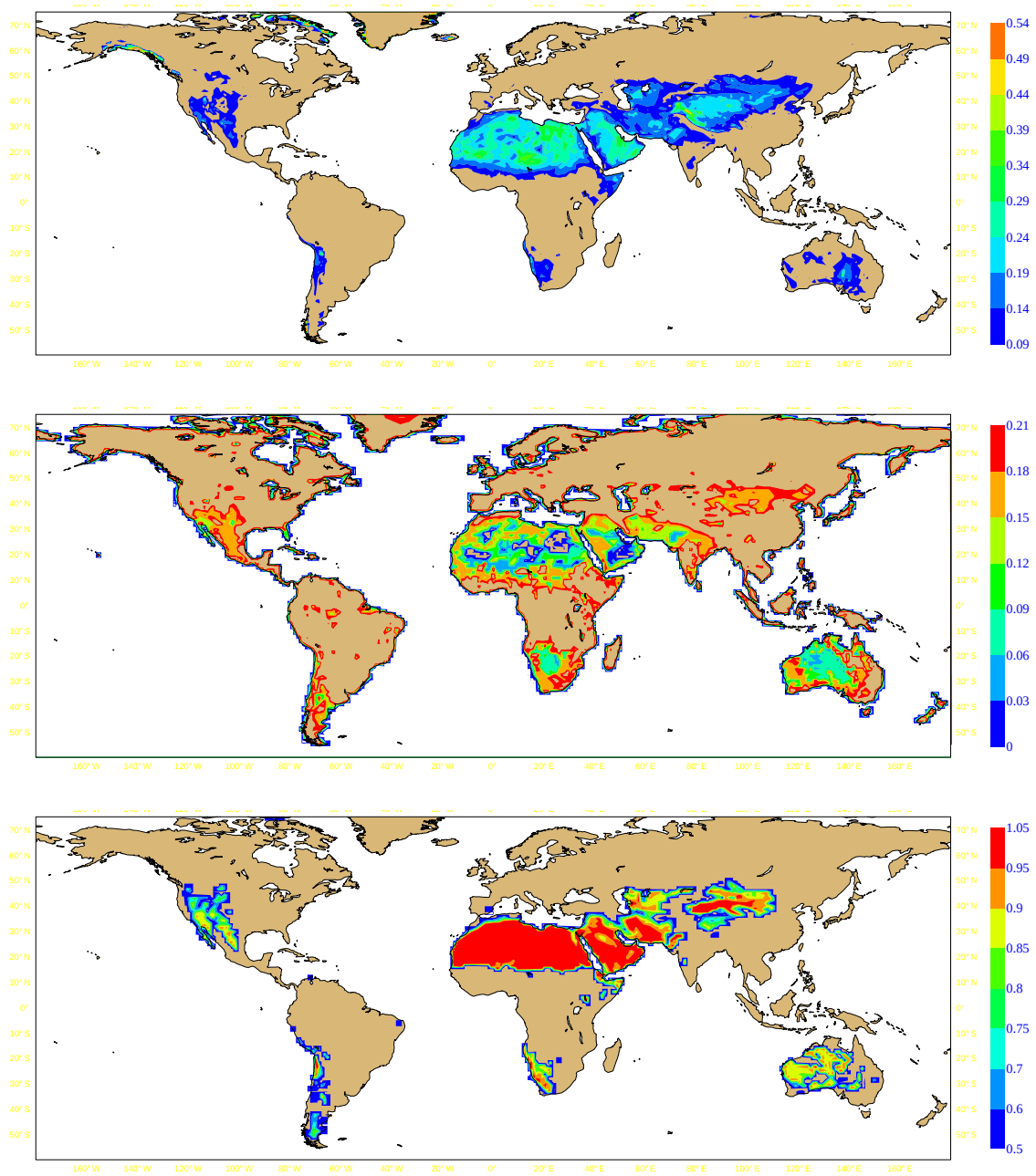

FIG. 4.
Top panel: The background albedo in the ultraviolet-visible part of the shortwave spectrum, for April 2003, from a snow-free climatology based on 2000-2004 observations. Only albedo with values between 0.09 and 0.54, assumed to be representative of light-coloured soil and sparse vegetation are plotted.
Middle panel: The soil moisture in the first layer of the ECMWF IFS model for April 2003.
Bottom panel: The fraction of bare soil for April 2003.

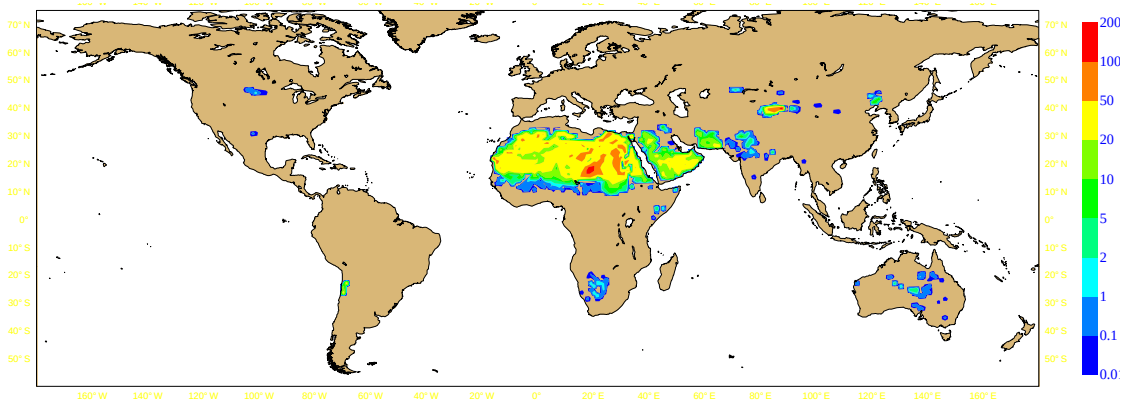

FIG. 5. The source of dust aerosols for April 2003 (in units of $gm^{-2}year^{-1}$).

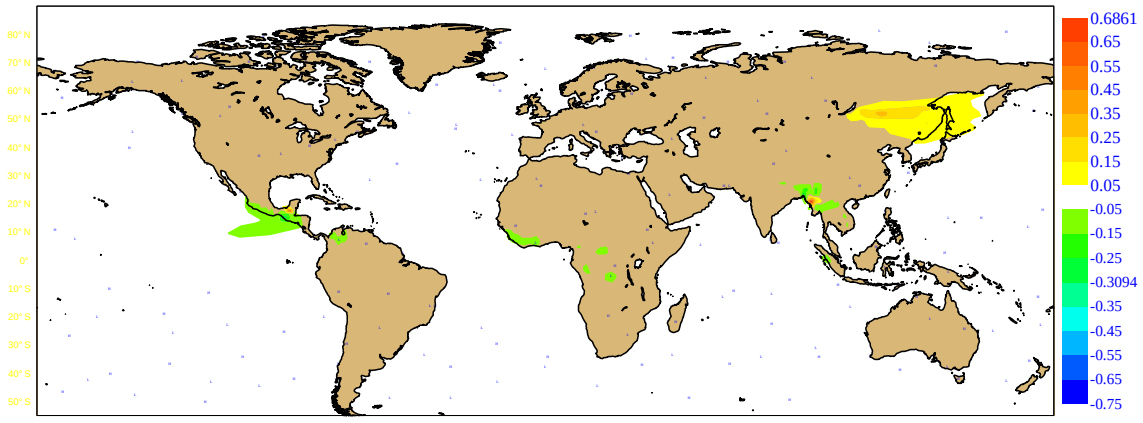

FIG. 6. The difference in aerosol optical depth at 550 nm for April 2003 using either GFEDv2 8-day or and GFED monthly climatologies for the sources of black carbon, organic carbon, and SO_4.

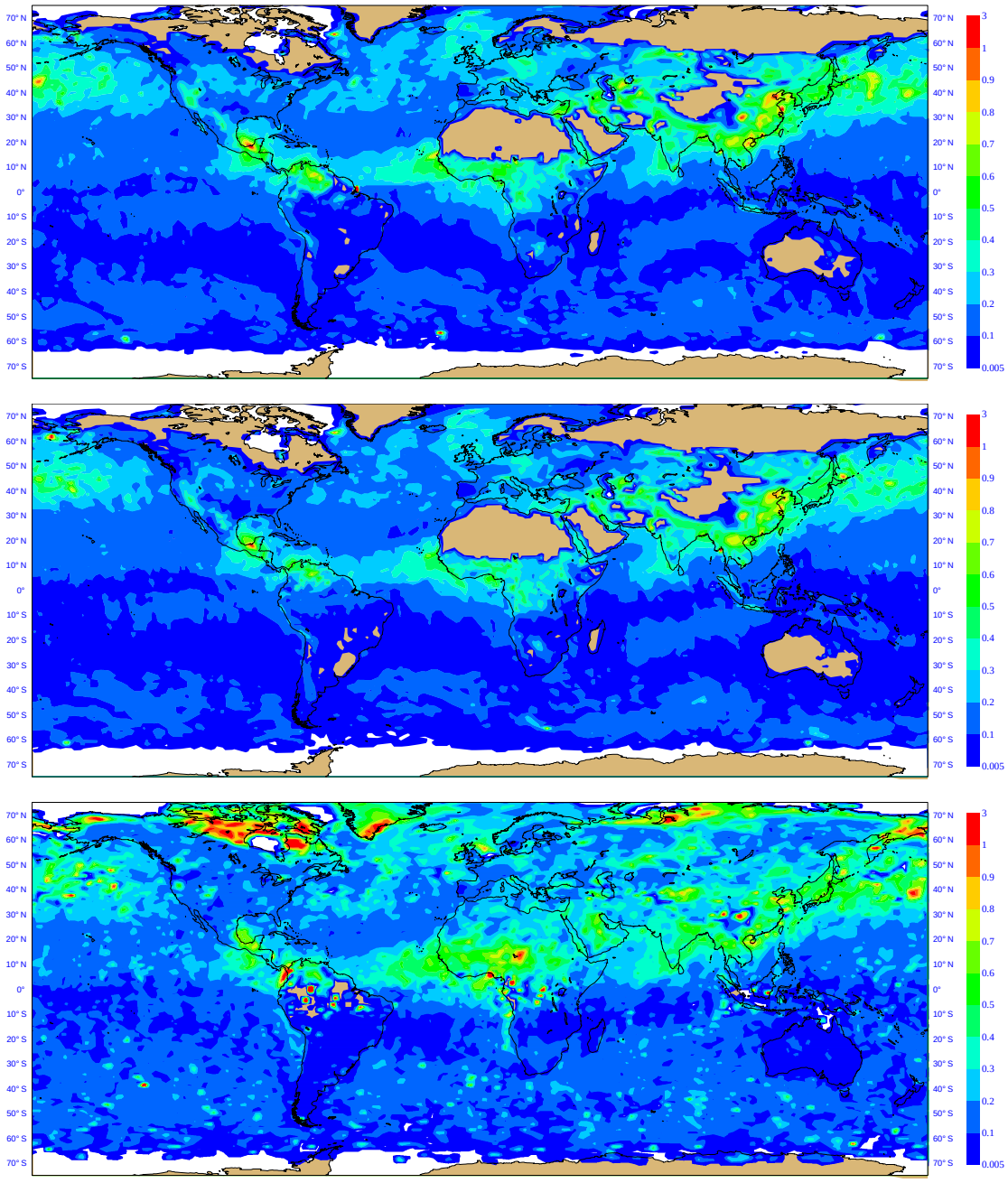

FIG. 7. The aerosol optical depth around 550 nm retrieved from satellite measurements for the months of April 2003. Top figure is the aerosol optical depth at 550 nm from MODIS on Terra, middle figure is the same quantity but from MODIS on Aqua. Bottom figure is the optical depth at 557.7 nm from MISR on Terra.

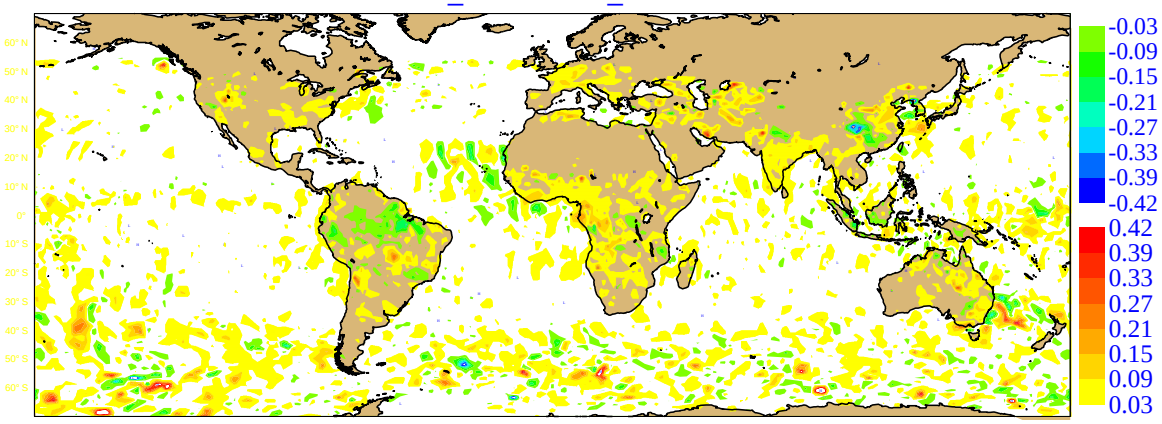

FIG. 8. The difference in aerosol optical depth at 550 nm (τ_{550}) derived from the MODIS measurements on-board the Terra and Aqua satellites, for April 2003.

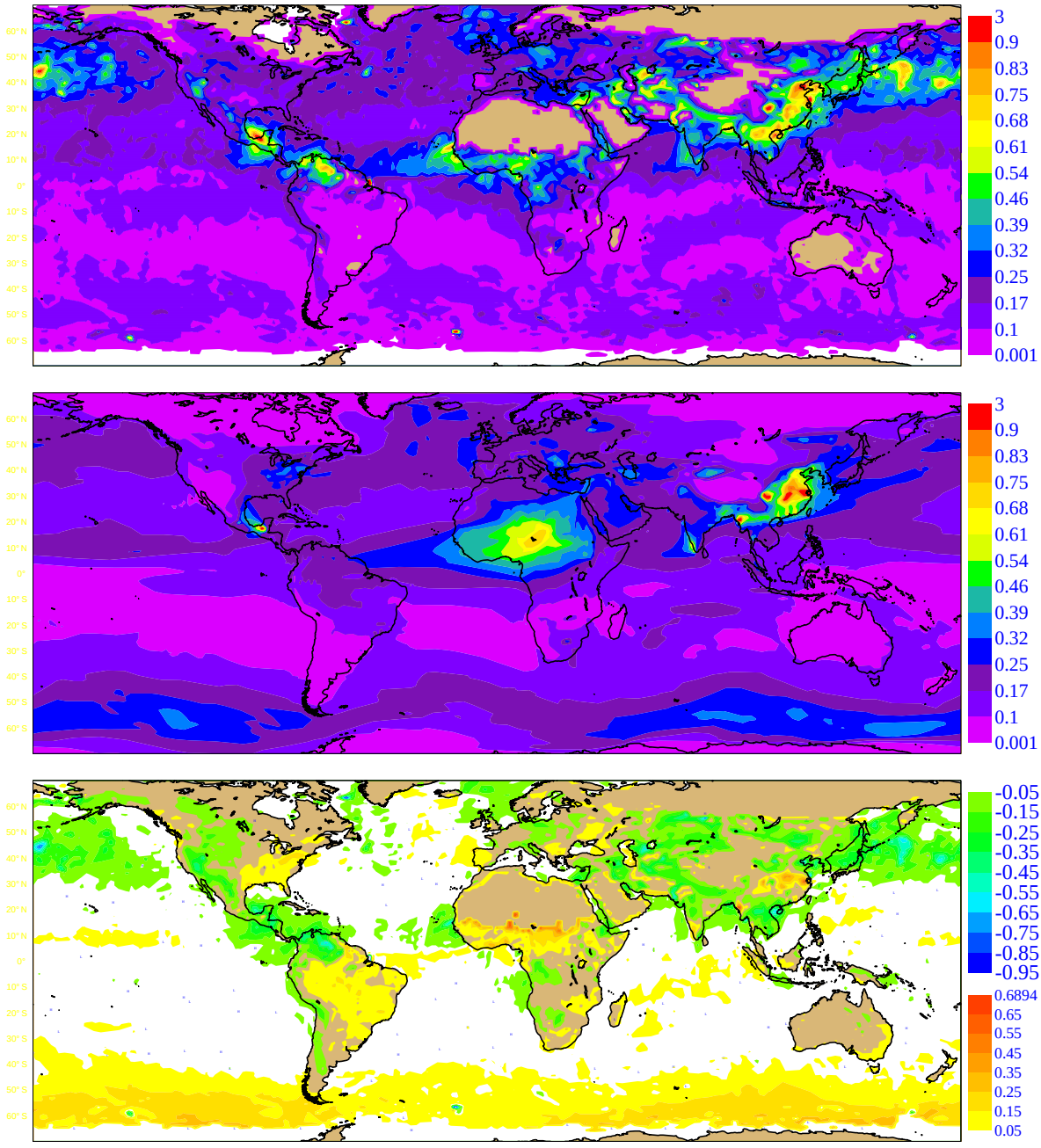

FIG. 9. The aerosol optical depth at 550 nm for April 2003 derived from the MODIS Terra satellite (top panel), from the ECMWF model (middle panel), and the difference ECMWF-MODIS (bottom panel).

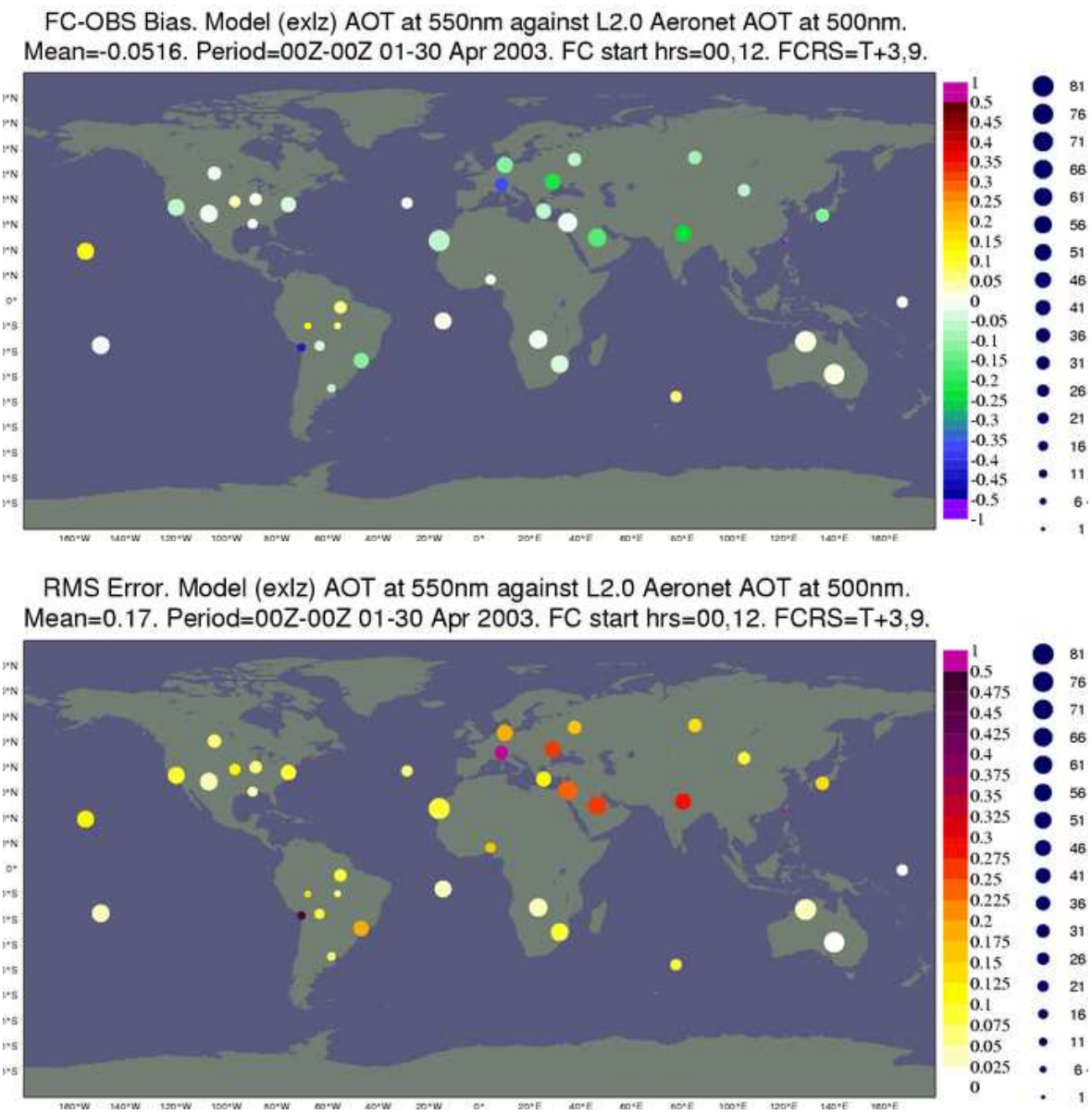

FIG. 10. Bias and r.m.s. error of the model aerosol optical depth at 550 nm against the AERONET observations at 500 nm for April 2003.

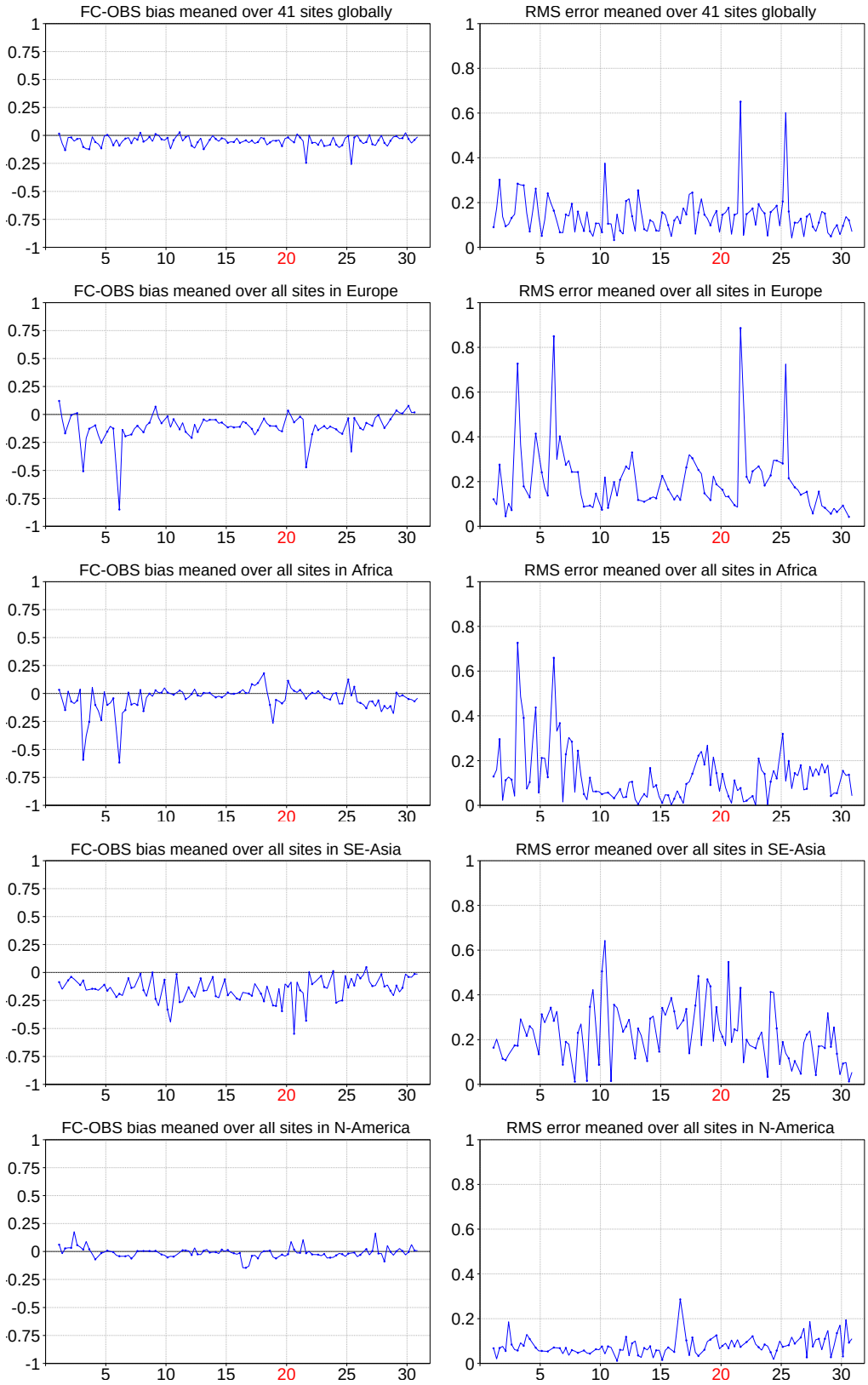

FIG. 11. Statistics of comparisons of the model τ_{550} with τ_{500} observed at AERONET stations for the 30 days of April 2003, over the globe, Europe, Africa, South-East Asia, and North America. Left column is the bias, right column is the r.m.s. error (non dimensional).

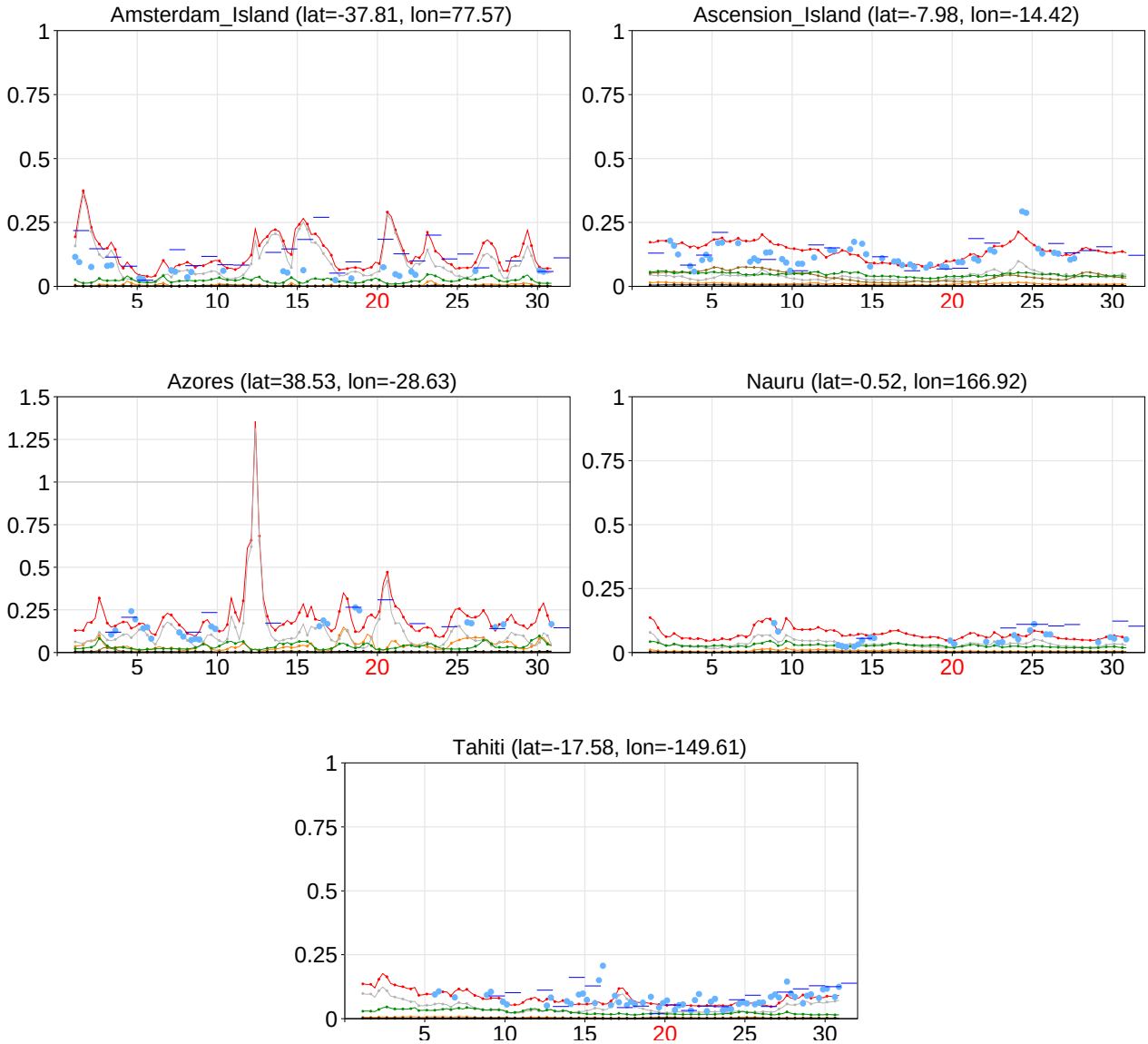

FIG. 12. Time-series of the optical depth at 500nm/550nm over five stations where sea salt aerosols are dominant. AERONET observations at 500 nm are given by blue-grey circles and MODIS τ_{550} by blue segments. The total model optical depth at 550 nm is in red. Other lines are for the various aerosol components: sea-salt (grey), dust (brown), organic carbon (green), black carbon (black), and sulphate (orange).

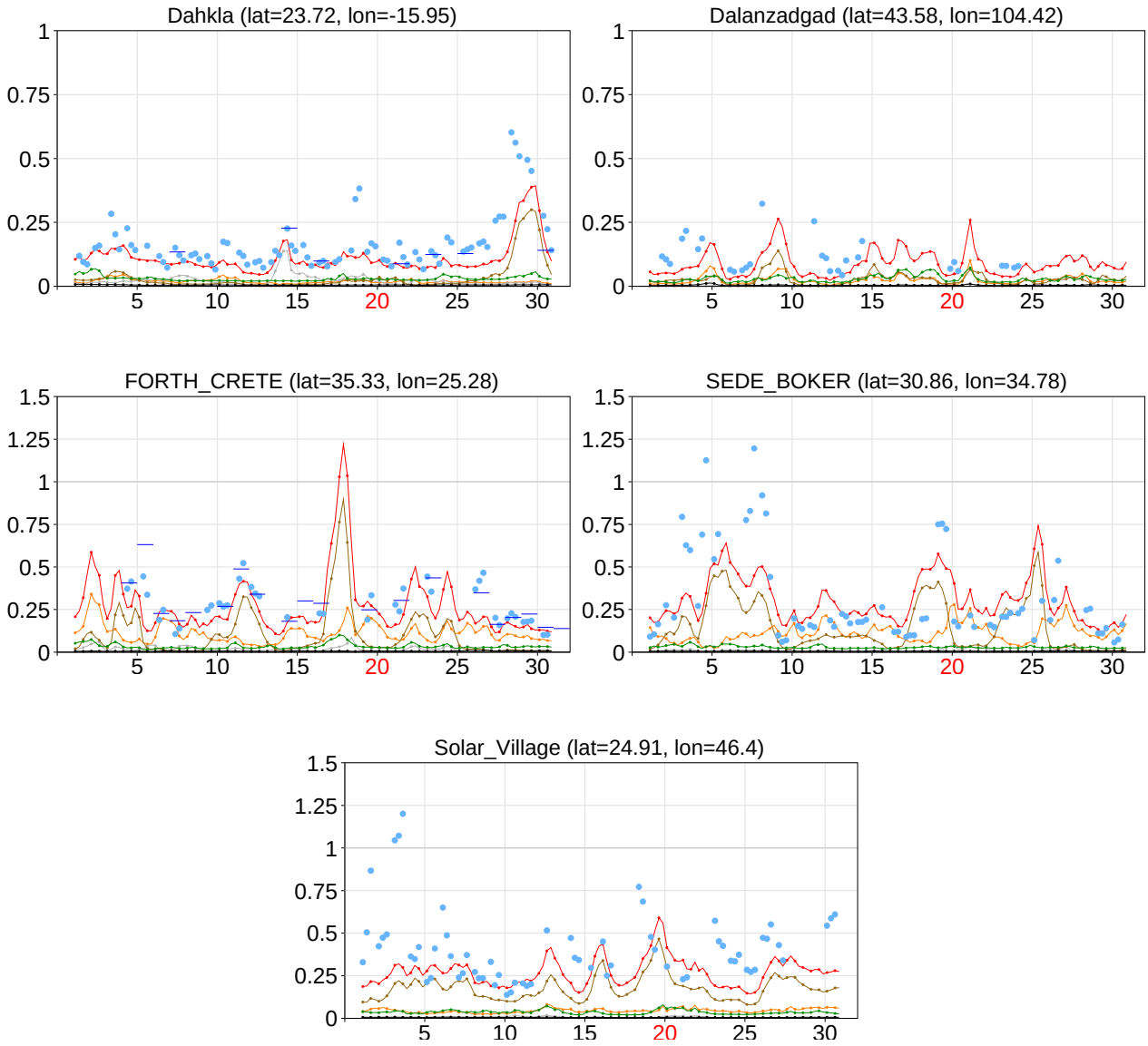

FIG. 13. As in Fig. 12, but for five stations where dust aerosols are prevalent.

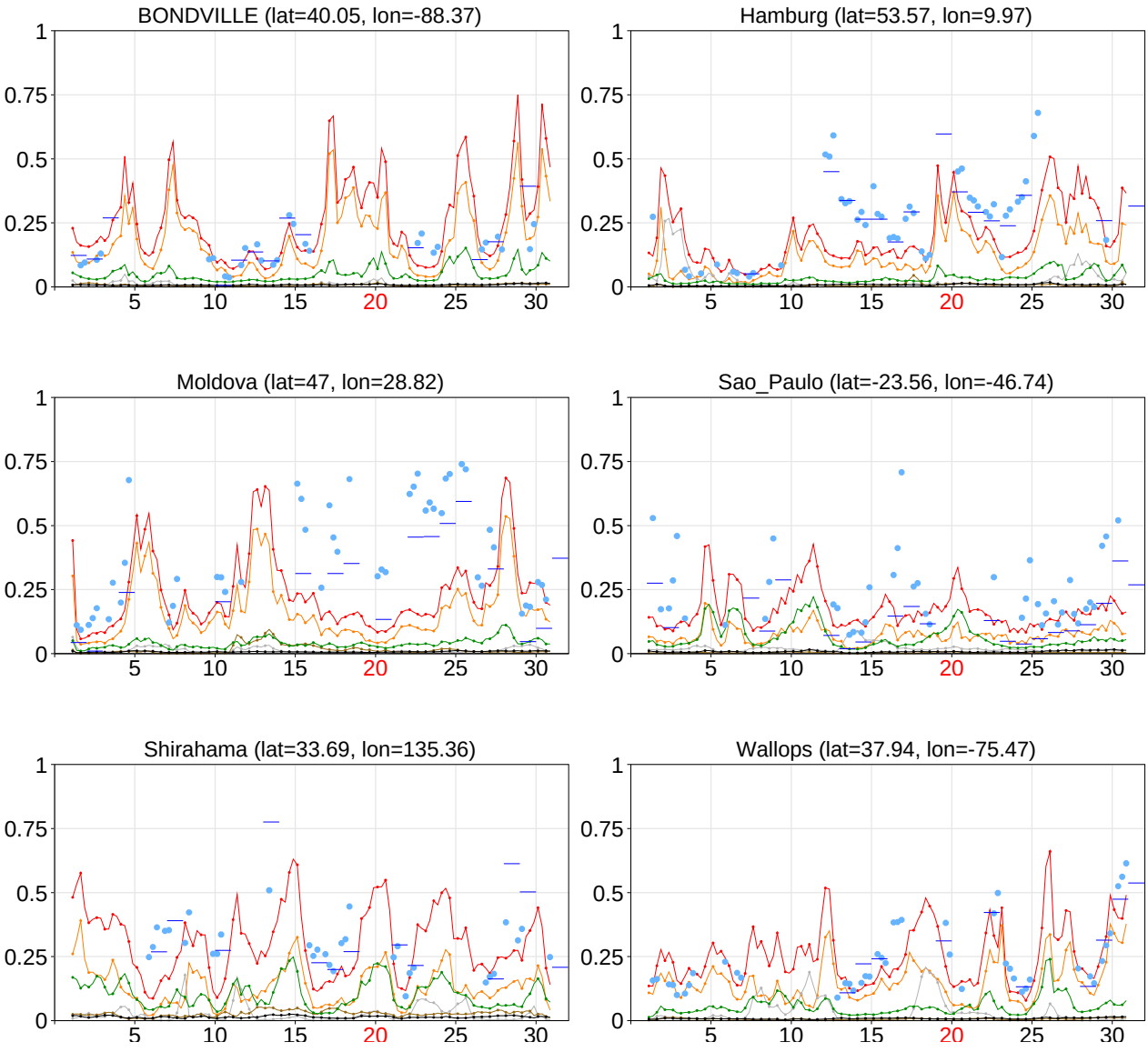

FIG. 14. As in Fig. 12, but for six stations where aerosols of anthropogenic origin are prevalent.

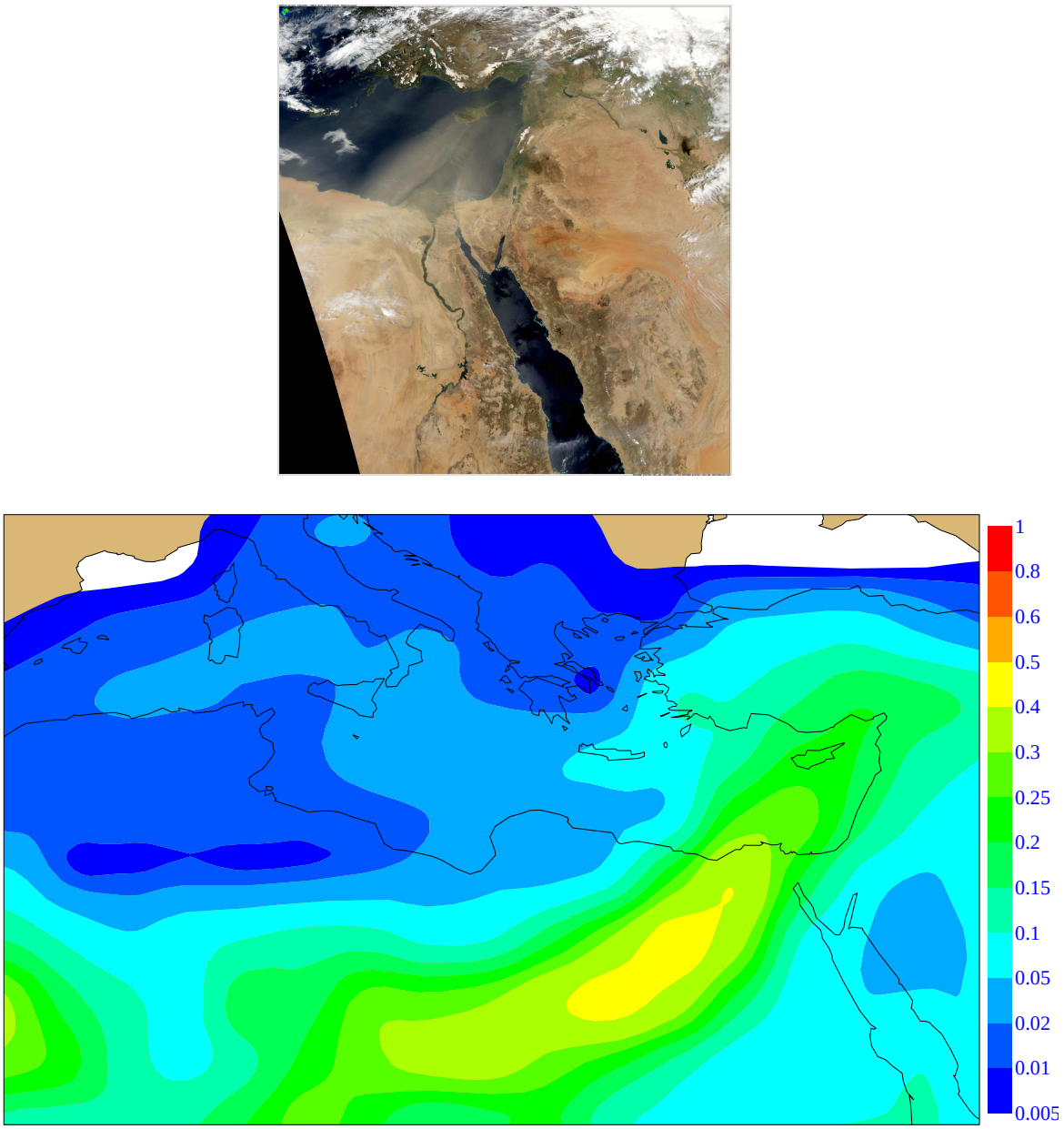

FIG. 15. Top: The MODIS imagery for a desert dust plume of aerosols on 4 April 2003. (courtesy, Louis Gonzalez, Laboratoire d'Optique Atmosphérique de Lille, France). Bottom: The corresponding optical depth at 550 *nm* for desert dust aerosols produced by the ECMWF forecasts started every 12 hours from operational analyses, and including prognostic aerosols, started from aerosol-free conditions on 1 December 2002 and cycling since that initial date.

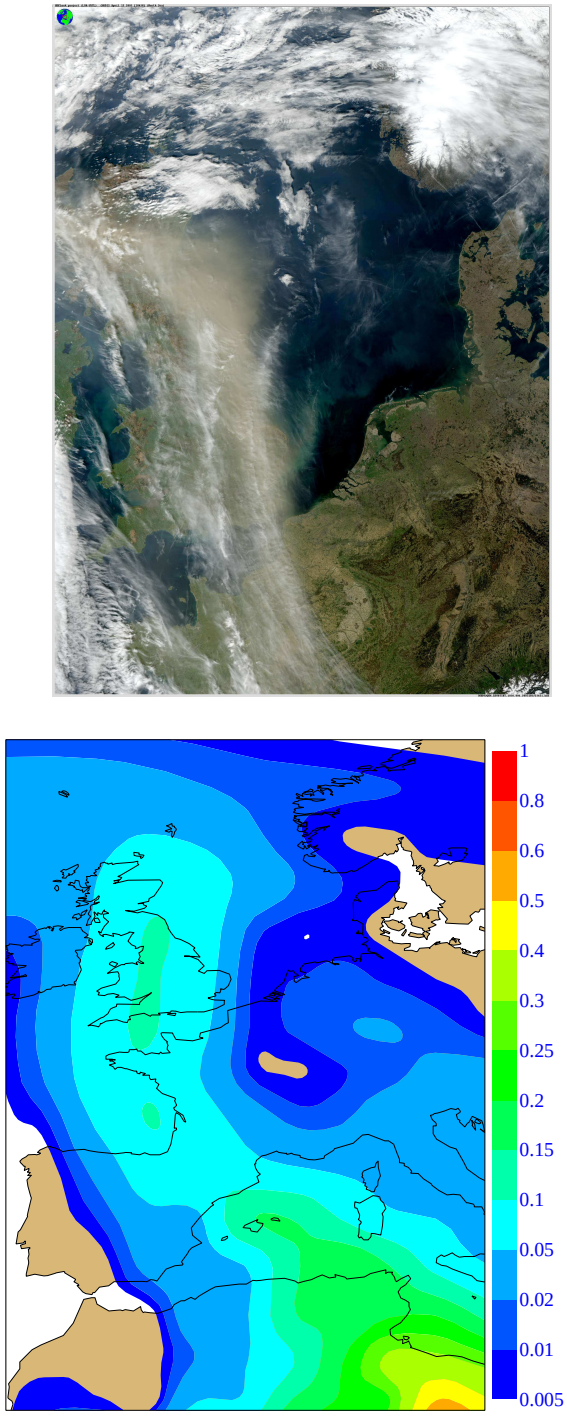

FIG. 16. As in Fig. 15, but for the optical depth at 550 *nm* for desert dust aerosols on 15 April 2003.

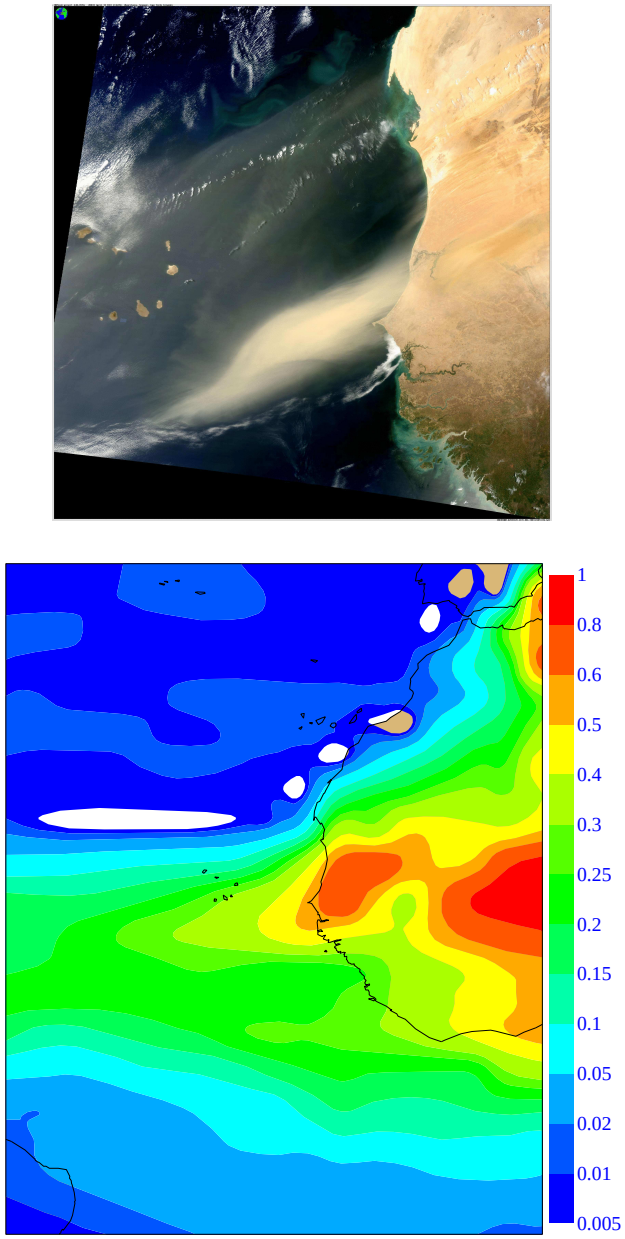

FIG. 17. As in Fig. 15, but for the optical depth at 550 *nm* for desert dust aerosols on 30 April 2003.

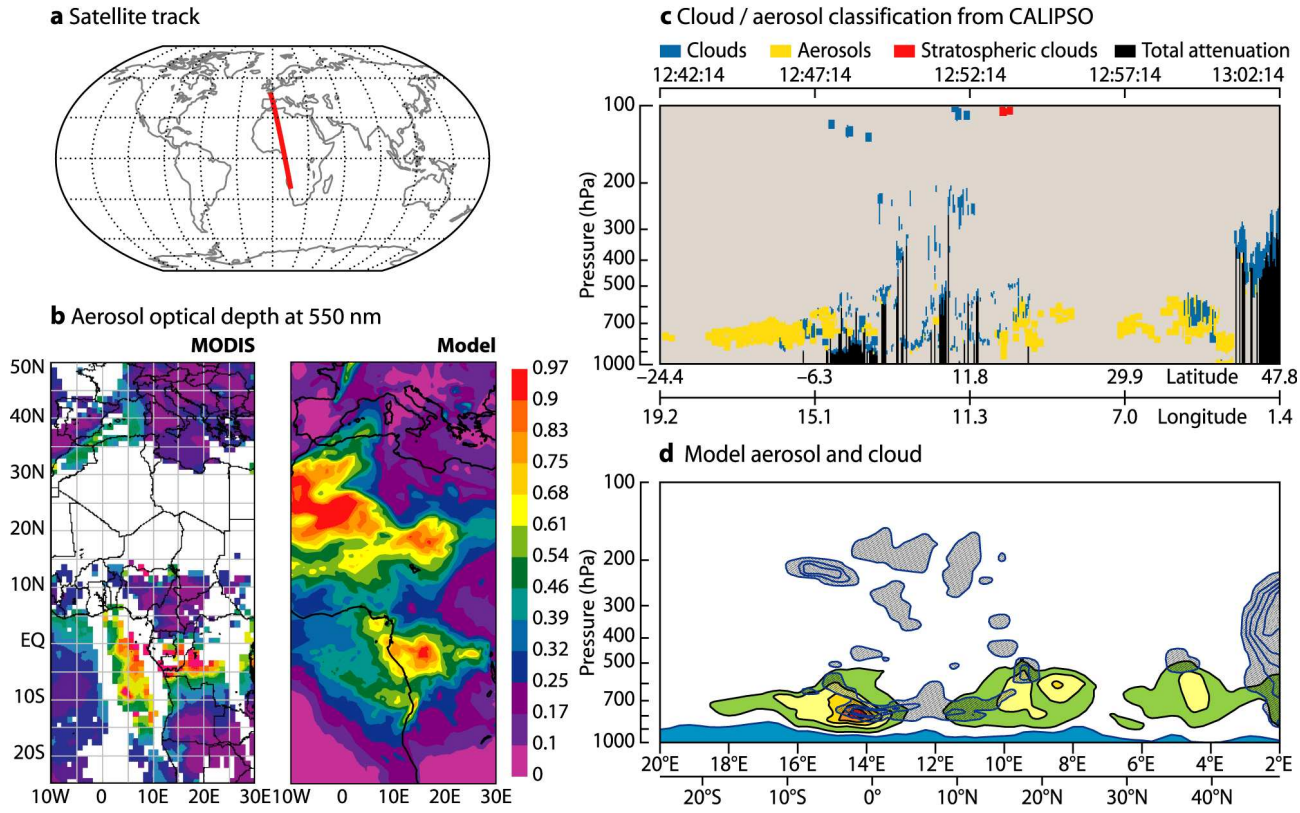

FIG. 18. (a) The orbit of the A-train of satellites on 16 July 2007 between 12:42 and 13:02 UTC.
(b) The aerosol optical depth at 550 nm derived from MODIS-Aqua observations (left) and produced by the ECMWF forecast model (right).
(c) The cloud/aerosol classification derived from CALIPSO measurements along the orbit shown in (a).
(d) The cross-section along the same orbit as used for (c) showing the aerosol (yellow/green) and cloud (grey) quantities produced by the ECMWF forecast model. The MODIS and CALIPSO data were downloaded from the NASA Giovanni server.

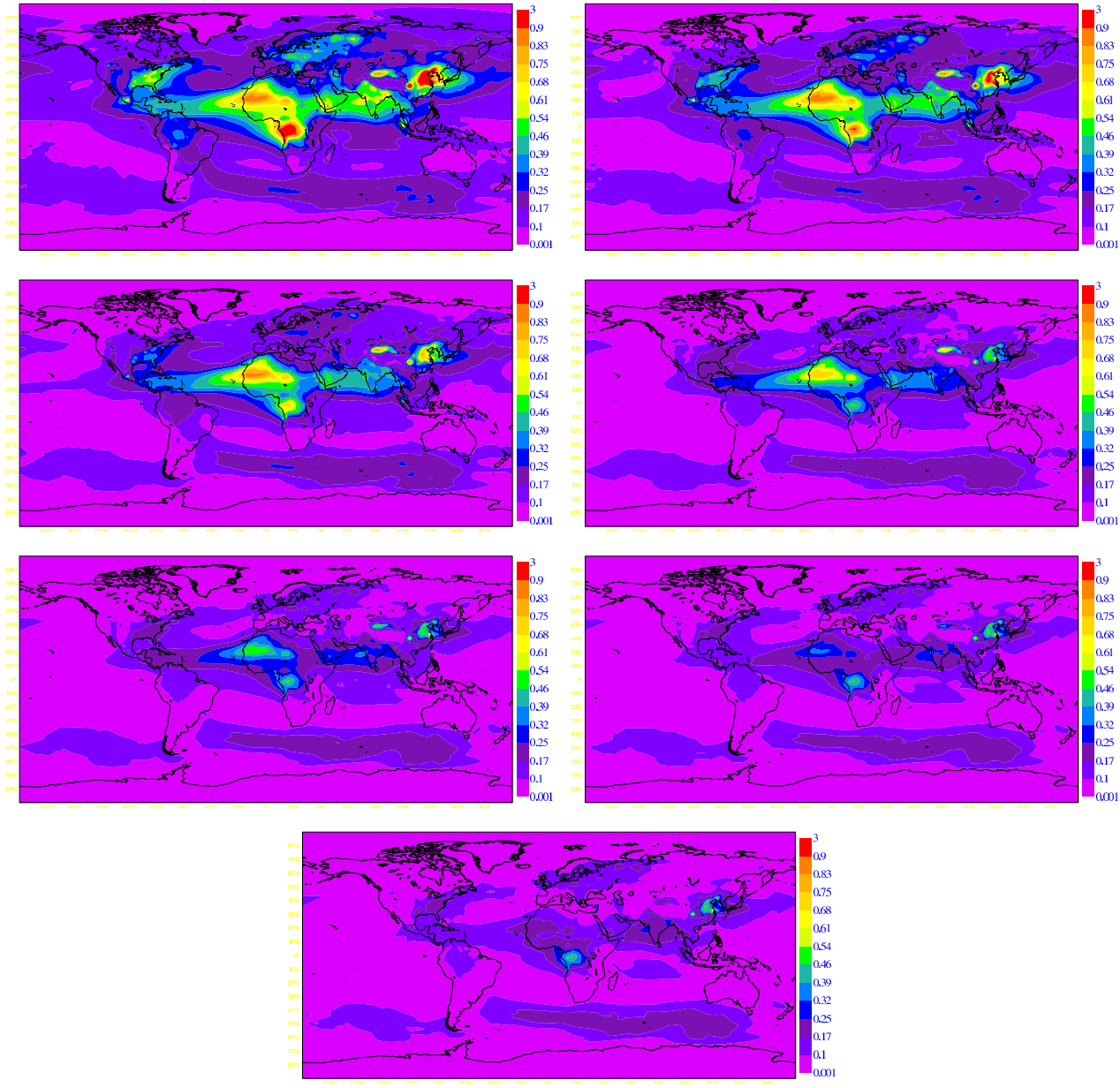

FIG. 19. The total optical depth for July 2007 produced by the ECMWF forecast including prognostic aerosols and simulated for the MODIS channels, from top to bottom, left to right, 469, 550, 670, 865, 1240, 1640 and 2130 *nm* respectively. Same forecast conditions as in Fig. 18 (see text).